TRIBHUVAN UNIVERSITY

INSTITUTE OF ENGINEERING

PULCHOWK CAMPUS

THESIS NO : 079MSMSE009

Synthesis and Characterization of Cobalt Cerium Co-doped Zinc Oxide Nanoparticles for Photocatalytic and Antimicrobial Applications

By

Madhusudan Adhikari

A THESIS

SUBMITTED TO THE DEPARTMENT OF APPLIED SCIENCES AND CHEMICAL ENGINEERING IN PARTIAL FULFILLMENT OF THE REQUIREMENTS FOR THE DEGREE OF MASTER OF SCIENCE IN MATERIALS SCIENCE AND ENGINEERING

DEPARTMENT OF APPLIED SCIENCES AND CHEMICAL ENGINEERING

LALITPUR, NEPAL

NOVEMBER, 2025

COPYRIGHT

BOARD OF EXAMINATION AND CERTIFICATE OF APPROVAL

This thesis entitled **"Synthesis and Characterization of Cobalt Cerium Co-doped Zinc Oxide Nanoparticles for Photocatalytic and Antimicrobial Applications"** by Madhusudan Adhikari (Roll No. PUL079MSMSE009 and T.U. Registration 8-2-41-124-2016) under the supervision of Asst. Prof. Dr. Deval Prasad Bhattarai, Department of Chemistry, Amrit Campus, Institute of Science and Technology, Tribhuvan University, and Co-supervision of Asst. Prof. Dr. Tanka Mukhiya in the Department of Applied Sciences & Chemical Engineering, Pulchowk Campus, Institute of Engineering, Tribhuvan University, is hereby submitted for the partial fulfilment of the Master of Science (M.Sc.) degree in Materials Science and Engineering. This report has been accepted and forwarded to the Controller of Examination, Institute of Engineering, Tribhuvan University, Nepal for the legal procedure.

Dr Deval Prasad Bhattarai
Supervisor
Department of Chemistry, Amrit Campus, Tribhuvan University, Nepal

Dr Tanka Mukhiya
Co-supervisor
Department of Applied Sciences and Chemical Engineering, Pulchowk Campus, Institute of Engineering, Tribhuvan University, Nepal

Prof. Dr Raja Ram Pradhananga
External Examiner
Department of Chemistry, Amrit Campus, Tribhuvan University, Nepal

Prof. Dr Sahira Joshi
Head of Department
Department of Applied Sciences and Chemical Engineering, Pulchowk Campus, Institute of Engineering, Tribhuvan University, Nepal

Date: November 25, 2025

RECOMMENDATION

This is to recommend that Mr. Madhusudan Adhikari (Roll No PUL079MSMSE009, T.U. Registration No.8-2-41-124-2016), has carried out the thesis work entitled "Synthesis and Characterization of Cobalt Cerium Co-doped Zinc Oxide Nanoparticles for Photocatalytic and Antimicrobial Applications" as part of the requirements for the Master of Science (M.Sc.) degree in Materials Science and Engineering under my supervision in the Department of Applied Sciences & Chemical Engineering, Pulchowk Campus, Institute of Engineering, Tribhuvan University, Kathmandu, Nepal.

He has fulfilled all the requirements laid down by the Institute of Engineering, Tribhuvan University, Nepal for the submission of the thesis work for the partial fulfillment of Master of Science (M.Sc.) degree in Materials Science and Engineering.

Supervisor
Dr. Deval Prasad Bhattarai
Assistant Professor of Chemistry
Department of Chemistry
Amrit Campus
Tribhuvan University

DECLARATION

This thesis entitled "**Synthesis and Characterization of Cobalt Cerium Co-doped Zinc Oxide Nanoparticles for Photocatalytic and Antimicrobial Applications**" is submitted to the Department of Applied Sciences & Chemical Engineering, Pulchowk Campus, Institute of Engineering, Tribhuvan University, Nepal for the partial fulfillment of the requirements for the Master of Science (M.Sc.) degree in Materials Science and Engineering. This thesis work is carried out by me under the supervision of Assistant Professor Dr. Deval Prasad Bhattarai, Department of Chemistry, Amrit Campus, Institute of Science and Technology, Tribhuvan University, Nepal.

This work is done by me originally and has not been submitted earlier, for the award of any other degree.

Madhusudan Adhikari
Roll. No. PUL079MSMSE009
T.U Reg. No. 8-2-41-124-2016

सर्वं श्रीकृष्णार्पणमस्तु

To

My Mom and Dad

Acknowledgement

I pay my sincere gratitude towards my supervisor Asst. Prof. Dr. Deval Prasad Bhattarai, and co-supervisor Asst. Prof. Dr. Tanka Mukhiya for their guidance, mentoring and motivation. I am also grateful towards Mrs. Purnima Mulmi and Mrs. Roshana Shrestha, Dr. Laxmi Thapa, Dr. Sunita Basnet for their support in the laboratory works during the experimentation. I would also like to express my gratitude towards Dr. Ganesh Shrestha, MSMSE program Co-ordinator and Head of the Department Prof. Dr. Sahira Joshi for their support and guidance throughout this journey. Additionally, I would like to acknowledge my colleague Mr. Saugat Chapagain for his technical and moral support throughout the course. I acknowledge the Department of Applied Sciences & Chemical Engineering, Pulchowk Campus and Department of Chemistry, Amrit Campus, Tribhuvan University, Nepal. A special thanks to Sancha Laxmi Tamang of the department who managed the availability of research labs throughout the research.

Madhusudan Adhikari

Abstract

This research investigates the synthesis and functional enhancement of zinc oxide (ZnO) nanoparticles through cerium (Ce) and cobalt (Co) doping for photocatalytic and antimicrobial applications. Pure ZnO, Ce-doped-, Co-doped-, and Ce–Co co-doped ZnO nanoparticles were synthesized via chemical co-precipitation method, followed by calcination at 500 °C. Physicochemical characterization was carried out via various characterization techniques. Optoelectronic properties were measured by using UV–Vis spectroscopy, surface morphology was studied using FESEM, and elemental detection of the prepared samples was carried using EDS, confirming successful dopant incorporation and morphological refinement. UV–Vis analysis revealed bandgap modulation with a slight red-shift for Ce and Ce–Co co-doped samples, while FESEM images showed reduced particle size and improved uniformity in co-doped systems. Photocatalytic performance was evaluated through methylene blue degradation under UV irradiation, where co-doped ZnO exhibited superior activity, achieving ~99.8% degradation within 120 minutes for the 0.25% Co + 1% Ce codoped sample. Antimicrobial assays against *Escherichia coli*, *Staphylococcus aureus*, and *Candida albicans* demonstrated enhanced inhibition zones for doped samples, with Ce–Co co-doped ZnO showing the strongest effect (up to 17 mm), comparable to standard antibiotics. The findings suggest that Ce–Co co-doping is an effective strategy to optimize ZnO for multifunctional applications in environmental remediation and biomedical fields.

Keywords: ZnO NPs, Co-Ce co-doping, Photocatalysis, Methylene blue, Antimicrobial activity

List of Tables

List of Figures

List of Abbreviations and Symbols

AFM – Atomic Force Microscope

CNT – Carbon Nanotube

DNA – Deoxyribonucleic Acid

DPPH – 2,2-Diphenyl-1-picrylhydrazyl

EDX – Energy-Dispersive X-ray Spectroscopy

LC_{50} – Median Lethal Concentration

MH / MHA – Mueller-Hinton / Mueller-Hinton Agar

NP / NPs – Nanoparticle(s)

RNA – Ribonucleic Acid

ROS – Reactive Oxygen Species

RSA – Radical Scavenging Activity

SEM / HR-SEM – Scanning Electron Microscope / High-Resolution SEM

STM – Scanning Tunneling Microscope

UV – Ultraviolet

XPS – X-ray Photoelectron Spectroscopy

XRD – X-ray Diffraction

ZnO – Zinc Oxide

ZOI – Zone of Inhibition

Table of Contents

Chapter 1 - Introduction

1.1 Background

The science and technology of manipulating matter at nanoscale, typically between 1 and 100 nanometres, is known as nanotechnology. At this scale materials display unique physical, chemical, and biological properties which are not observed at larger scales. Phenomena like quantum confinement and enhanced surface to volume ratios dominate at this scale providing space for the development of novel structures with improved or new functionalities (McNeil, 2005). Invention like Scanning Tunneling Microscope (STM), Atomic Force Microscope (AFM) and discovery of carbon allotropes like fullerenes, carbon nanotubes and graphene have provided tools and materials that has shaped materials science into a vibrant interdisciplinary field incorporating physics, chemistry, biology and engineering (Schiavo et al., 2024).

A transformative role is played by nano technology in medicine with targeted drug delivery and bio sensors, in environment science through water treatment and pollution remediation and in energy systems via fuel cells, supercapacitors, solar energy conversion and hydrogen storage. Nanotechnology has a strong place in biology because many natural structures like protein, enzymes, DNA, RNA and viruses are naturally occurring at the nanoscale making them an ideal area for nanoscale systems, for example carbon nanotubes are noted for their versatile usage in biomedical applications like scaffolds, bioelectronics, biosensors and bio implants. In addition to that, nanoscale biosensors based on CNT can detect DNA hybridization, antigen recognition, and enzyme reaction with appreciable sensitivity. Furthermore, nanostructures have been shown to be both non-toxic and cytocompatible. Features like these have placed nanotechnology in such a place where it expands the possibilities for diagnostics, therapy and biomedical engineering (Nasrollahzadeh et al., 2019).

Another area where nanotechnology has a strong potential is industrial pollution degradation through photocatalysis. The expansion of sectors such as textiles, pharmaceuticals, agriculture, pulp and paper, metal plating and food processing, has led to the discharge of substantial quantities of persistent organic and inorganic contaminants into the environment which has

become a major global concern. Most of these discharges contain low-biodegradable compounds like synthetic dyes, pesticides, and antibiotic residues. These pollutants resist natural degradation and get accumulated in soil, surface water, and ground waters. These accumulations lead to long term ecological damage and pose a significant threat to human and aquatic lives. Remediation techniques that are available traditionally are not able to eliminate these persistent pollutants, leading to growing interest in more effective ways such as advanced oxidation processes and photocatalytic technologies (Geldasa et al., 2023).

For degrading pollutants that are resistant to other methods, photocatalysis has proven to be highly effective. In contrast to traditional oxidation processes, photocatalysis can fully degrade dyes and chemicals into carbon dioxide (CO_2) and water (H_2O), even breaking down stable compounds that are otherwise tough to remove. Under normal temperature and pressure, it works efficiently without needing a special oxygen supply. In terms of cost effectiveness, photocatalysis is cost effective and generates no waste disposal issues, turning it to a better alternative to other oxidation methods (Zhang et al., 2018).

A category of materials identified as highly promising photocatalytic material is metal oxide nanoparticles. They have distinctive semiconducting, electronic, and surface properties. At nanoscale, with their large surface areas, they have enhanced charge transfer characteristics, enabling the efficient generation of electron hole pairs under irradiation of light. These charge carriers generated through light irradiation, called excitons, initiate redox reactions that produce ROS, capable of mineralizing stable organic pollutants, dyes and other industrial wastes (Geldasa et al., 2023).

One of the most extensively studied nanomaterials is Zinc Oxide (ZnO), which is characterized by its chemical stability, biocompatibility, and broad-spectrum antimicrobial and photocatalytic activities. Furthermore, ZnO shows improved surface reactivity and unique photocatalytic behavior at nanoscale. It also generates ROS and releases zinc ions that inhibit microbial growth alongside maintaining comparatively low toxicity towards mammalian cells. Its photocatalytic behavior is driven by the interplay of semiconducting properties, defect-chemistry and surface interactions. With excitations through UV and visible light, electron hole pairs are produced which progress to the oxidative degradation process. Additionally, structural and compositional

modification which includes hierarchical morphologies, impurity doping, metal deposition and integration with carbon-based materials improve charge separation, widen the optical absorption and increase the reactive sites. With all these features, ZnO nanoparticles are tunable and efficient materials with significant potential across biomedical and environmental applications (Sushma & Kumar, 2017).

ZnO is an inorganic, semiconducting material whose nanostructures have gained attention for applications in electronics, optoelectronics, cosmetics, food packaging, and biomedical science. ZnO nanostructures' antimicrobial activity is mainly due to the generation of specific ROS such as hydrogen peroxide, hydroxyl radicals, and superoxide anions, in addition to direct interaction with the cell membrane of microorganisms. These mechanisms lead to bacterial cell-wall damage, disruption of membrane integrity, and leakage of intracellular contents, ultimately causing cell death. ZnO NPs have shown effective results against both Gram-positive and Gram-negative bacteria, with *Staphylococcus aureus* and *Escherichia coli* being among the most widely studied. The efficiency of antimicrobial activity is highly dependent on particle size, concentration, and structure, with smaller particles exhibiting stronger bactericidal effects due to increased ROS generation (Ijaz et al., 2020; Kumar et al., 2017).

Along with antibacterial material, ZnO NPs have also emerged as a strong antifungal material. ZnO NPs show their antifungal effects by attaching them to fungal cell walls, interacting with functional groups like amides and polysaccharides, and generating ROS including hydrogen peroxide, hydroxyl radicals, and superoxide anions. These ROS damage cell membranes, disrupt hyphae, and compromise overall cell integrity, ultimately leading to fungal death (Sharma & Ghose, 2014; Ahmad et al., 2022).

Pure ZnO has a wide band gap of 3.35 eV and high exciton binding energy of 60meV and strong photocatalytic potential. But applications like photocatalysis, optoelectronics and sensing changes in its structure and band gap are necessary. Doping is one of the mechanisms to introduce those changes. Doping in nanostructured materials involves the intentional incorporation of impurity ions into a host lattice to tune its properties. Concentrations vary widely: sub-1 mol% is common in hosts with small cationic sites, while rare-earth fluorides such as $NaYF_4$ can accommodate up to 60 mol% without major structural changes. Doping is defined

by its functional purpose rather than a fixed percentage, ranging from trace levels to near-complete substitution to achieve desired optical, magnetic, or catalytic properties (Zheng et.al, 2022).

Doping modifies ZnO's structural, optical, magnetic, and catalytic behavior. Different dopants introduced by various synthesis procedures change properties of ZnO for specific applications. For example, doping with Ag reduces band gap and reduces electron-hole recombination, Cu doping improves dye degradation, Mg doping introduces ferromagnetism (Bharat et al., 2019). On photocatalytic performance of ZnO, research has consistently shown that doping ZnO with various metal ions changes its electronic structure, defect density and light absorption behavior resulting in a significant change in photocatalytic activity. An emphasis on incorporating transition metals like Fe, Co, Ni, Cu, or Mn and rare earth ions like Ce, Gd, or La or other dopants introduce impurity energy levels within the ZnO band gap. These incorporations narrow the effective bandgap and enable improved visible light absorption. The dopants also modify the defect morphology particularly oxygen vacancies and interstitial zinc which play a central role in charge-carrier trapping and separation. These changes reduce electron hole recombination rate. Metal incorporation can also stabilize photogenerated carriers, improve surface adsorption of pollutants and in some cases even suppress photo corrosion depending on the doped metal's oxidation state and ionic radius (Sushma & Kumar, 2017).

For antimicrobial properties, doped ZnO nanoparticles have shown a marked improvement over pure ZnO, depending strongly on the type and concentration of dopant. Antibacterial property is already present in pure ZnO because of its ability to generate ROS such as hydroxyl radicals and superoxide ions which disrupt bacterial membranes and proteins. But doping with metals like Manganese, Iron, Cobalt and many more further changes crystal size, band gap, and surface properties of ZnO, leading to greater ROS production and stronger bactericidal activity (Sharma et al., 2016; Premanathan et al., 2015).

With these diverse properties and usages of pure and doped ZnO nanostructures, it is essential to investigate their synthesis, characterization, biological, and photocatalytic activity. Most of the existing research focuses on single-metal doping or rare-earth doping individually. For co-doping

strategies combining transition metals like cobalt (Co) with rare-earth elements such as cerium (Ce) remain limited. There is a lack in current literature in comprehensive analysis of how synergistic effects of Ce and Co co-doping bring on photocatalytic efficiency and antimicrobial performance simultaneously. This gap motivates research on structural, optical, and functional modifications brought by Ce–Co co-doping in ZnO NPs. Also, their correlation with improved photocatalytic dye degradation and antimicrobial activity is not available as in the case with other co-doping experiments found in the literature.

Regarding the mechanism of doping, in classical semiconductor physics, doping generally refers to the introduction of trace amounts of impurities, typically in the range of parts per million to atomic percent. However, within the context of nanomaterials, the term doping is more broadly applied to the incorporation of foreign ions at molar-percent levels. But during this incorporation the host lattice should remain largely intact. In such cases, dopants influence material properties through mechanisms such as defect-chemistry and solid-solution formation. Numerous studies and reviews consistently classify additions of 1–10 mol% of rare-earth or transition-metal ions to oxide nanocrystals as doping. In those studies, there were significant modifications in band structure, defect states, morphology, and catalytic behavior, while preserving the fundamental wurtzite ZnO framework (Zheng et.al, 2022). Maier (2017) further emphasizes that even relatively high impurity concentrations may still be considered doping, as long as the ideal lattice structure remains approximately invariant. This convention has been widely adopted in ZnO photocatalysis research and in reviews of rare-earth-doped nanocrystals.

In this research photocatalytic properties of doped and co-doped ZnO nanoparticles have been studied by taking Methylene Blue(MB) as a representative industrial dye. The schematic chemical reaction involved in the photocatalytic phenomenon is

$$\mathrm{MB\,(aq) + ZnO\,(s) + h\nu \longrightarrow degradation\ products\ (CO_2, H_2O, etc.)}$$

Photocatalytic dye degradation occurs due to the generation of ROS. Initially Photoexcitation of ZnO happens leading into production of electrons and holes.

$$\mathrm{ZnO + h\nu \rightarrow\ e_{cb}^{-} + h_{vb}^{+}}$$

The electrons and holes lead to the formation of ROS species like,

Hydroxyl radicals

$$h_{vb}^{+} + H_2O_{(ads)} \rightarrow \cdot OH + H^{+}$$

$$h_{vb}^{+} + OH_{(ads)}^{-} \rightarrow \cdot OH$$

Superoxide radicals

$$e_{cb}^{-} + O_2 \rightarrow O_2^{\cdot -}$$

Hydrogen Peroxide

$$O2^{\cdot -} + H^{+} \rightarrow HO_2^{\cdot}$$

$$2HO_2^{\cdot} \rightarrow H_2O_2 + O_2$$

These ROS attack the methylene blue molecule, eventually mineralizing it to CO_2, H_2O, and inorganic ions.

Along with photocatalytic activity on MB, antimicrobial properties of the prepared nanomaterials on gram negative bacteria, gram positive bacteria and fungus have been studied in this research along with their cytotoxicity and radical scavenging property.

1.2 Research questions

This research is driven by following questions

1. How do co-doping ZnO NPs with Ce and Co affect and alter their structural and morphological characteristics in comparison to pure ZnO ?
2. To what extent does Ce–Co co-doping improve the photocatalytic degradation capacity of Methylene Blue under UV irradiation compared to pure Ce doped ZnO?
3. How does Ce–Co co-doping affect the antimicrobial and antifungal activity of ZnO nanoparticles against Gram-positive bacteria, Gram-negative bacteria, and fungi?

1.3 Objectives

To address the research questions, the developed objectives of the thesis are mentioned in terms of general objective and specific objectives as follows:

1.3.1 General objective

Preparation of Ce doped, Co doped and Ce and Co co-doped ZnO nanoparticles and study its photocatalytic, antibacterial and antifungal properties.

1.3.2 Specific objectives

- Preparation of ZnO by coprecipitation method
- Doping of ZnO nanoparticles with Ce, Co and codoping with both of them.
- Characterization of the prepared nanomaterials.
- Study of photocatalytic degradation of Methylene Blue by the prepared nanoparticles
- Study of antimicrobial properties of the prepared nanoparticles on *E.Coli*, *Staphylococcus aureus*, and *Candida albicans*.
- Study of cytotoxicity on Nauplii
- Study of radical scavenging Activity

1.4 Significance of the study

Water pollution is a serious problem for both terrestrial and aquatic lives. NPs with capacity to degrade industrial pollutants as well as perform antimicrobial activity can deal with both chemical and biological factors polluting water. Another application area of such nanoparticles is with coating technology. To protect various materials from fungal and bacterial growth, they can be coated with antimicrobial nanoparticles. In the biomedical sector, antimicrobial materials have a significant place because they can be used as alternatives to traditional antibiotics or as a supporting material for synergistic outcomes. In this study both photocatalytic and antimicrobial properties have been studied. Also, optimization of dopants is being carried out. These functionalities can be utilized in water pollution mitigation, antimicrobial coatings, and biomedical applications.

1.5 Organization of the dissertation

The dissertation has been organized in the following manner.

Chapter 1 is the introduction and objective

Chapter 2 discusses the literature review

Chapter 3 presents the materials, methods and experiments

Chapter 4 presents the results and discussion

Chapter 5 presents conclusion

Chapter 2 - Literature Review

Nanotechnology has a broad scope in dozens of impactful domains and has the potential to revolutionize medicine, agriculture, environmental protection, and industry. In agriculture, nanotechnology has extended itself through smart fertilizers and pesticide delivery systems. For soil and crop monitoring, nano sensors are utilized. Disease-resistant plants are developed through nanotechnology. In environmental applications, water purification, pollution control, and bioremediation utilize nanomaterials to remove toxins and heavy metals. In the industrial domain, improved food processing and packaging, energy production and novel material design, nanotechnology is heavily utilized. It is transforming the biomedical sector with quantum dots and nanoparticles, enhancing diagnostics through highly sensitive biosensors and imaging technologies. With nanocarriers like liposomes, dendrimers, and polymeric nanoparticles targeted, drug delivery with reduced side effects is being achieved. In therapeutics with therapies like hyperthermia and photodynamic therapy, nanomaterials precisely destroy cancer cells. Nanoscale scaffolds are used in tissue and bone regeneration. Nanoscale tools have allowed manipulation and detection of DNA and proteins at unprecedented resolution (Klefenz, 2004).

Nanomaterials in the biomedical sector have opened broad possibilities for diagnostics and therapy and utilizing their properties observed at nanoscale. They have ultra small size, large surface to volume ratio and tunable optical and magnetic features which are used in designing of biosensors, boosting imaging and precisely delivering drugs. Gold, silver, and carbon nanomaterials are the backbones of biosensing systems which have allowed the detection of biomolecules and pathogens with high sensitivity. In imaging, fluorescence and MRI contrast are improved by nanoparticles and in detection and elimination of microbes and cancer cells they play a dual role of both detectors and eliminators. Drug delivery systems which are built upon materials like liposomes, polymeric carriers, mesoporous silica and functionalized ZnO nanorods enable controlled and targeted release of drugs even across the barriers. In tissue engineering, hydroxyapatite, calcium phosphates and CNT-based scaffolds along with mimicking natural bone structure, improve mechanical strength. Nanoparticles are found to support hyperthermia which is utilized in generating heating to kill tumors and photodynamic therapy where light activated

particles agitate ROS species which is utilized in killing cancer cells. These examples show their promising position in transformation of medicine (Das et al., 2013).

Another important side of nanoparticles are their properties as antibacterial agents. Traditional organic compounds used for antibacterial purposes have limitations due to their toxicity and fast development of bacterial resistance. In contrast, inorganic nanoparticles have different physiochemical properties like high surface to volume ratios and reactive surface that make them interact with bacterial cells in fundamentally different ways. The shortcomings of these traditional antibacterial drugs can be overcome by these attributes. There is a strong influence of physical and structural characteristics possessed by nanoparticles when it comes to their interaction with bacteria. In Gram-positive bacteria there is a thick peptidoglycan layer full of teichoic acids and in Gram-negative bacteria there is a thinner wall shielded by an additional external membrane with lipopolysaccharides. How particles penetrate and act on bacterial cells is determined by these variations. Also, bacterial growth has an impact on vulnerability. Rapidly growing bacteria are more sensitive to nanoparticle action in comparison to slow growing bacteria which develop tolerance. Additional blockades are formed by biofilms, complex bacterial communities enclosed in extracellular polymers. Despite these blockades, certain nanoparticles like magnesium fluoride and zinc oxide can damage biofilm formation and restore antibacterial efficacy. The underlying mechanism for nanoparticle induced toxicity towards bacteria is multidimensional. Nanoparticles generally attach to bacterial membranes through electrostatic interactions, leading to structural damage and leakage of cellular contents. The central phenomenon is the generation of ROS, which causes oxidative stress that leads to DNA damage, protein oxidation, and lipid peroxidation. The acting mechanisms of different materials are different, for example titanium dioxide and zinc oxide display photocatalytic activity under ultraviolet light, the toxicity of copper oxide is affected by pH and aeration conditions, silver nanoparticles attack bacteria on multiple sides leading to damage of membranes, binding with genetic material and enhancing the effectiveness of antibiotics when used in synergy. Another key strength of nanoparticles is their ability to target antibiotic-resistant bacteria. Formulations like silver carbene complexes, and hybrid structures combining immunoglobulins with titanium dioxide have shown activities against multidrug-resistant strains. With urgent clinical challenges where conventional antibiotics have failed, nanomaterials have the potential to address the need.

Intriguing results of nitric oxide releasing nanoparticles and zinc oxide nanoparticles exhibiting potent effects against resistant species, including methicillin-resistant *Staphylococcus aureus potent effects against resistant species, including methicillin-resistant Staphylococcus aureus* have shown the promising place of nano particles in tackling the modern medical problem of antibiotics resistance (Hajipour et al., 2012).

Along with bacterial infections, fungal infections present a significant global health concern. From superficial skin infections to invasive and life-threatening systemic diseases, fungal infections have a diverse impact on the human body. Existing antifungal therapies have some critical issues which include poor solubility in water, high levels of toxicity, and emergence of resistance in fungal strains. Nanotechnology, as with the case of antibacterial treatment, has a significant place for antifungal activity as well. Nano particles are not just the passive carriers, but themselves are antifungal by nature depending on their material composition. This dual capacity puts nanoparticles at the frontline of future antifungal treatment.

A variety of nanoparticles have been studied for their antifungal properties. Metal and metal oxide nanoparticles like silver, zinc oxide, titanium dioxide, and copper oxide have shown strong antifungal properties. By disrupting the fungal cell wall and membrane, generating reactive oxygen species, and interfering with important cellular processes, these materials act against the fungi. Other types of nanoparticles, polymeric nanoparticles, on the other hand, provide encapsulation for convenient antifungal drugs like amphotericin B and fluconazole. For the improvement of the therapeutic effect, these systems improve solubility and reduce toxicity and also enable sustained and controlled drug release. Examples of improvement in drug stability and absorption can be taken that of lipid-based systems which includes liposomes, solid lipid nanoparticles, and nanostructured lipid carriers. These lipid-based systems mimic biological membranes, thereby improving drug absorption and stability. Another example can be taken of carbon-based materials like graphene oxides and carbon nanotubes which show antifungal action by physically piercing cell membranes. This piercing not only damages the membranes but also serves as delivery systems for antifungal compounds. Nanoparticles showing antifungal effects is a multidimensional phenomena. One of the mechanisms is the damaging of the cell wall and membrane structure compromising cell viability. Another mechanism is the production of ROS

leading to the induction of oxidative stress and damaging of important biomolecules such as DNA, proteins, and lipids. They also interfere with basic biological functions like DNA replication and protein synthesis. Another important property is their ability to damage fungal biofilms. These biofilms are dense protective layers which generally protect fungal cells from existing therapies. Nanoparticles, by breaking through these protections, improve drug effectiveness while treating persistent infections (Niemirowicz et al., 2017).

Improving the efficiency of nanomaterials is another major area of research in the field which looks into well-balanced design, functionality, and adaptability. Among many strategies, one is surface functionalization which involves attaching biomolecules, polymers, and ligands to the surface of nanoparticles. Along with improvement in stability and dispersability in the biological environment, this method improves the ability of nanoparticles to selectively target bacterial cells with minimized harm towards mammalian cells. With fine tuning of the surface properties, precision and reliability of nanomaterials as antibacterial agents is increased. Another critical factor which impacts the efficiency of nanomaterials is their size, shape, and morphology. With reduction in particle size, the surface to volume ratio of the particles is increased. This increment strengthens their interaction with bacterial membranes. Similarly, specific shapes such as rod-like particles and sharp-edged graphene sheets have the ability to disrupt and pierce bacterial cell walls more effectively. Even small changes in crystallinity of metal oxides like zinc oxide or titanium dioxide can significantly improve the generation of ROS, increasing their bactericidal power. Synergy with antibiotics also gives efficiency to nanomaterials. As a carrier, they can deliver antibiotic molecules to the exact location of infection, overcoming the bacterial resistance. They also reduce the required drug dosage. With targeted delivery, not only antibiotic effectiveness is restored, but systemic side effects are mitigated. In parallel, eco-friendly and biocompatible nanoparticles are produced through green synthesis methods. These methods produce nanoparticles that have improved stability, reduced aggregation, and safer nature for medical and environmental applications. Green synthesis methods utilize natural extracts and microbial processes. Development of hybrid and composite nanomaterials is a powerful approach to improving performance. The combination of two or more materials such as silver with zinc oxide and parallel exploitation of multiple antibacterial mechanisms is possible. These hybrids demonstrate synergistic effects with coupling of ion release with oxidative stress or

physical disruption, leading to the achievement of results greater than the individual parts. Creation of stimuli responsive nanomaterials is further advancement in their efficiency. These materials show their antibacterial properties in response to environmental triggers like pH, light, and temperature. An example we can take is titanium dioxide and zinc oxide which show dramatic increments in production of ROS under UV and visible light (Yougbaré et al., 2021).

Doping in nanomaterials is a powerful strategy to change its properties, which are not possible with bulk materials. With an introduction of a small number of foreign atoms or dopants in the host lattice, the behavior of the material can be altered significantly. In nanostructures, even a single dopant atom can have a big influence in the properties because of small size and quantum confinement effects. This is why doping is considered a prominent method to achieve desired modifications. For metal oxides, doping is an approach to flexibly controlling the properties of materials. While preserving high surface to volume ratio of nanoparticles, adjustment in electronic structure, shifting of absorption into visible spectrum, increment in luminescence and improvement in photocatalytic activity can be achieved with doping. The effects of doping are multifaceted. In the electronic level, it can alter the bandgap by widening or narrowing it and also change the charge carrier behavior. Optically, it can shift absorption to visible range, change color, and change the intensity of photoluminescence. With suppression of electron-hole recombination, efficient use of excitons can be achieved which enhances photocatalytic and photochemical processes (Chen et al., 2005).

Doping metal oxides with rare earth ions like La^{3+}, Gd^{3+}, Nd^{3+}, Dy^{3+}, are considered effective because they introduce f-orbital states within the band structure. Rare earth dopants generally produce narrower band gaps, making ZnO active in the visible light region. Also, rare earths are able to boost the generation of hydroxyl radicals which are effective for both dye degradation and antimicrobial activity. Kumar et al. (2018) doped ZnO with dysprosium Dy^{3+} because the ionic radii are comparable to Zn3+ (Dy^{3+} = 0.091 nm vs. Zn^{2+} = 0.083 nm), allowing it to substitute into the ZnO lattice with minimum distortion. Also, its f-orbitals can act as electron traps, delaying recombination, and improving photocatalysis. The study was based on a co-precipitation method. In the study, the band gap was successfully reduced from 3.16 to 3.07 eV. This improved visible light absorption eventually caused photocatalytic dye degradation. In

terms of antimicrobial performance, the doped material showed superior antimicrobial performance in comparison to pristine ZnO. Manikandan et al. (2017) reported that significant changes in the crystal structure and particle morphology were achieved with doping of La^{3+}. Confirmation of all samples maintaining a hexagonal wurtzite structure was done through XRD analysis. A shift in diffraction peaks toward higher 2θ values, leading to slight distortion of the lattice, was caused by incorporation of La. But it did not disrupt its symmetry. With an increase in La content, the average crystallite size decreased. The crystallite size of pure ZnO was about 15.64 nm and for the highest La-doped sample (0.07M), the size reduced to 10.18nm. HR-SEM further confirmed the findings by showing sphere-like nanoparticles whose size decreased progressively with La concentration. The elemental composition was validated using EDX. In addition to the structural and optical effects, La doping significantly influenced the antibacterial performance of ZnO nanoparticles. A strong antibacterial activity against human pathogens *Proteus mirabilis* and *Salmonella typhi* was observed which are linked to kidney stones and typhoid fever. With increment in La concentrations, inhibition zones increased, reaching up to 22 mm for P. mirabilis at the highest doping level. Surprisingly, the material showed no significant effect against *Staphylococcus aureus* and *Bacillus subtilis*.

In another work Samarium was doped in ZnO. Ravi et al. (2024) investigated the influence of samarium (Sm) doping on the structural, optical, and antibacterial properties of ZnO nanorods synthesized through a simple wet chemical method followed by annealing at 400 °C, 500 °C, and 600 °C. Due to their favorable ionic size and electronic configuration, rare earth metals, particularly Sm^{3+}, are considered effective dopants, that incorporate into the ZnO lattice efficiently. In their work, the authors introduced 1 mol% Sm^{3+} into the ZnO system, ensuring a controlled modification of the material's properties without severe lattice distortion. The retention of the hexagonal wurtzite structure across all samples was confirmed through the analysis of X-ray diffraction. A noticeable peak shift indicating lattice expansion due to Sm substitution was analyzed. The most favorable crystallinity with smaller crystallite size and higher lattice strain was achieved in the 500 °C specimen among the three annealed samples. TEM revealed well-defined rod-like morphologies with average dimensions of about 132 nm in length and 31 nm in width. EDS and XPS confirmed the successful incorporation of Sm^{3+} into the ZnO lattice. Raman spectroscopy further supported these findings. Testing antibacterial

activity against both gram positive (*Staphylococcus aureus*) and Gram-negative (*Escherichia coli*) bacteria demonstrated a significant bactericidal activity was demonstrated by Sm-doped ZnO nanorods. The same 500 °C specimen produced inhibition zones of 20 mm against *E. coli* and 18 mm against *S. aureus*. The enhanced antibacterial effect was attributed to the generation of reactive oxygen species such as hydroxyl radicals, hydrogen peroxide, and superoxide anions, which disrupt bacterial membranes and damage DNA.

According to the review by Shukla and Sharma (2020), the doping of cerium (Ce) and erbium (Er) ions bring significant changes to both the structure and performance of ZnO nanostructures. Introducing Ce or Er into ZnO lattice changes the crystal growth mechanisms due to the larger ionic radius and different charge states of the rare-earth ions compared to Zn^{2+}. A noticeable morphological modification is reached by this like ZnO nanorods transforming into nanoplates when doped. Such structural changes are not just the confirmation on incorporation of rare-earth ions into the lattice but also the creation of new defect sites such as oxygen vacancies, interstitials, and dislocations which highly impact the ZnO's functional properties. Performance wise, doping of Ce introduces 4f–5d transitions that contribute to broad and tunable visible emissions. An improvement in ZnO's photoluminescence behavior is shown by this transition. Also, a reduction in band gap, enhancement in UV absorption and generation of additional defect states happens which support applications like photocatalysis, environmental remediation and sensing. A better performance on dye degradation, optical filtering and electron mediator in chemical sensing has been reported for Ce-doped ZnO. On the other hand, Er doping enriches ZnO with sharp intra-4f transitions, making it highly suitable for telecommunication and optoelectronic devices. It improves visible-light absorption, modifies the optical band gap, and enhances photocatalytic efficiency under visible irradiation.

Er doping also induces or strengthens room-temperature ferromagnetism in ZnO nanostructures. This expands their applications into magneto-optical and spintronic devices. Thus, by tuning the band gap, photoluminescence, magnetic ordering, and catalytic activity, Ce and Er doping make ZnO nanostructures more versatile. Their potential for usage of optoelectronics, photovoltaics, sensing, photocatalysis, and advanced device technologies is further increased by this.

For antibacterial studies against *Escherichia coli, Pseudomonas aeruginosa,* and *Staphylococcus aureus by* Senthil et al. (2020). It is revealed that Ce doping strengthens antibacterial activity. They observed the largest inhibition zones at 5% doping. The factor behind this enhancement is both due to the release of Zn^{2+} ions, which damage bacterial cells, and the increased ROS production. Overall, the study concludes that 5% Ce doping is the optimal concentration.

Multiple studies have been done on doping cobalt with ZnO. Oves et al. (2015) report that cobalt doping significantly influenced both the structural and antimicrobial properties of zinc oxide (ZnO) nanoparticles. For pure ZnO, a crystalline wurtzite phase with rod-like morphology was present which with introduction of cobalt changed to more spherical particles which was confirmed by SEM and XRD analysis. A slight increment in crystallite size from 20.5 nm of pure ZnO to 25.7 nm of 5% Co-doped ZnO was observed. Also, the bandgap widened from 3.22 eV to 3.30 eV indicating electronic structure modification. For antibacterial efficiency with already a notable activity of pure ZnO, further boosting was achieved with cobalt doping, leading to increment in bactericidal effect by 22-33% against waterborne pathogens such as *Shigella dysenteriae, Salmonella typhi, Vibrio cholerae,* and *Escherichia coli*. Stronger interactions with bacterial membranes were possible due to smaller effective particle size and increased surface-to-volume ratio of Co-doped ZnO. Moreover, sunlight exposure further amplified this effect, reducing the minimum bactericidal concentration from 80–60 µg/ml in pure ZnO to 50–30 µg/ml in 5% Co-doped ZnO. So cobalt incorporation's effect was observed not only on ZnO's structural characteristics but also on its antimicrobial behavior, particularly in photocatalytic conditions.

Along with doping cerium, multiple studies have been done previously on co-doping cerium and other metals over zinc oxide. Subash et al. (2013) in their research co-doped silver and cerium over zinc oxide. Co-doping zinc oxide with silver (Ag) and cerium (Ce) led to notable structural and functional modifications that enhanced its photocatalytic performance. XRD and TEM showed reduced crystallite size and well-dispersed hexagonal ZnO particles. XPS confirmed the presence of surface metallic Ag^0 and Ce^{4+}. The dopants extended light absorption into the visible region, suppressing electron hole recombination by trapping charge carriers. Oxygen reduction was facilitated by Ag capturing conduction band electrons and Ce^{4+} undergoing Ce^{3+}/Ce^{4+} cycling. These effects enabled higher production of reactive oxygen species, resulting in

superior degradation of Reactive Red 120 dye under sunlight compared to pure or singly doped ZnO.

Significant structural and functional modifications have been shown by Co-doping of ZnO nanoparticles with lanthanum (La^{3+}) and cerium (Ce^{3+}). According to Al Al Bitar et al. (2023), the crystalline ZnO wurtzite structure was preserved after co-doping, but secondary phases of La_2O_3 and CeO_2 emerged due to incomplete substitution of Zn^{2+} ions. TEM revealed that while pure ZnO nanoparticles exhibited a distorted hexagonal morphology with an average size of around 70 nm, the co-doped samples demonstrated a dual size distribution of around 72 nm and around 10 nm.This indicates improved control over morphology. The functional implications of these structural changes were evident in antimicrobial activity. While pure ZnO nanoparticles were highly effective against gram-negative bacteria such as *Escherichia coli* and *Klebsiella pneumoniae*, the La–Ce co-doped samples shifted their spectrum of activity toward gram-positive strains. Co-doped nanoparticles specially showed potent inhibitory effects against *Staphylococcus aureus* and *Staphylococcus haemolyticus.* A unique suppression in the growth of *Streptococcus intermedius* was observed which showed resistance to other tested samples.These findings highlight co-doping with La and Ce not only alters the structural characteristics of ZnO nanoparticles but also broadens their antimicrobial efficacy.

Chapter 3 - Materials and Methods

3.1 Materials and Equipment

The following materials and equipment were used in the preparation of nanoparticles.

3.2.1 Chemicals

The following chemicals were used in the synthesis of nanoparticles.

Zinc Nitrate Hexahydrate ($Zn(NO_3)_2 \cdot 6H_2O$(Qualigens, Mol mass 297.48, Assay 96-103 %),

Cobalt Nitrate Hexahydrate ($Co(NO_3)_2 \cdot 6H_2O$ (Qualigens, Mol mass 297.48, Assay 97-101 %)

Cerium Nitrate Hexahydrate ($Ce(NO_3)_3 \cdot 6H_2O$ (Sigma Aldrich, Mol. mass 434.22, Assay 99.999%)

Aqueous Ammonia (Fizmerk, 32%)

Methylene Blue (Loba Chemie)

Ethanol (99.99% RCP Distilleries)

All of the nitrate salts were of analytical grade, and no further processing was done. They were used as obtained

3.2.2. Equipment

Commonly used equipment to conduct the experiment are magnetic stirrer (Gallenkamp), oven (Gallenkamp), muffle furnace (Scarlet Alloys Wire), etc.

3.3 Preparation of Nanoparticles

Zinc oxide nanoparticles undoped, cerium-doped, cobalt-doped, and cerium–cobalt co-doped were all synthesized using chemical co-precipitation methods. For undoped ZnO, the required amount (as presented in Table 1) of zinc nitrate hexahydrate was dissolved in approximately 250 mL of distilled water, to prepare 0.1M of zinc nitrate solution, under magnetic stirring. For the doped systems, the appropriate quantities of zinc nitrate hexahydrate together with cerium nitrate hexahydrate, cobalt nitrate hexahydrate, or both (for co-doped samples) (all as presented in Table-1) were accurately weighed and dissolved in 250 mL of distilled water to obtain homogeneous precursor solutions. For Ce and Co co-doped samples, a fixed molar percentage of

0.25% was maintained for Co salts. Variations were done only on the Ce percentages similar to the mono-doped samples. After the addition of salts, the solution was stirred with a magnetic stirrer for 1 hour for uniform mixing of the metal salts.

While stirring, ammonium hydroxide solution was added dropwise to each precursor mixture until a slightly alkaline pH of 7-8 was achieved, leading to the controlled co-precipitation of zinc hydroxide. The resulting precipitates were collected by filtration and thoroughly washed several times with distilled water and then by ethanol to remove residual ions. The washed hydroxides were then dried and calcined in a muffle furnace at 500 °C for 5 hours to form undoped or doped ZnO nanoparticles. Finally, all calcined products were ground into fine powders using a mortar and pestle to ensure uniformity and improve dispersibility for subsequent characterization.

Table 1: Weights of Salts of Zinc and Dopants for the preparation of samples

Sample Code	Sample Type	Ce (mol%)	Co (mol %)	$Zn(NO_3)_2 \cdot 6H_2O$ (g)	$Ce(NO_3)_3 \cdot 6H_2O$ (g)	$Co(NO_3)_2 \cdot 6H_2O$ (g)
ZnO	Undoped ZnO	0	0	7.4374	–	–
Ce(0.5)-ZnO	Ce-doped ZnO	0.5	0	7.4374	0.0543	–
Ce(1)-ZnO	Ce-doped ZnO	1	0	7.4374	0.1086	–
Ce(3)-ZnO	Ce-doped ZnO	3	0	7.4374	0.3257	–
Ce(5)-ZnO	Ce-doped ZnO	5	0	7.4374	0.5428	–
Co(0.25)-ZnO	Co-doped ZnO	0	0.25	7.437		0.114
Co(0.5)-ZnO	Co-doped ZnO	0	0.5	7.437		0.228
CoCe(0.5)-ZnO	Ce–Co co-doped ZnO	0.5	0.25	7.4374	0.0543	0.0114
CoCe(1)-ZnO	Ce–Co co-doped ZnO	1	0.25	7.4374	0.1086	0.0114
CoCe(3)-ZnO	Ce–Co co-doped ZnO	3	0.25	7.4374	0.3257	0.0114
CoCe(5)-ZnO	Ce–Co co-doped ZnO	5	0.25	7.4374	0.5428	0.0114

The salts were calculated such that for a fixed concentration of 0.1 M zinc nitrate solution, the dopant salts were added according to the molar percentages shown in Table 1. For example, in the 0.5% Ce mono-doped sample, 250 mL of 0.1 M zinc nitrate solution was prepared by dissolving 7.437 g of zinc nitrate hexahydrate in distilled water. To this solution, 0.0543 g of cerium nitrate hexahydrate was added, corresponding to 0.5 mol% of the moles of zinc nitrate present in the solution.

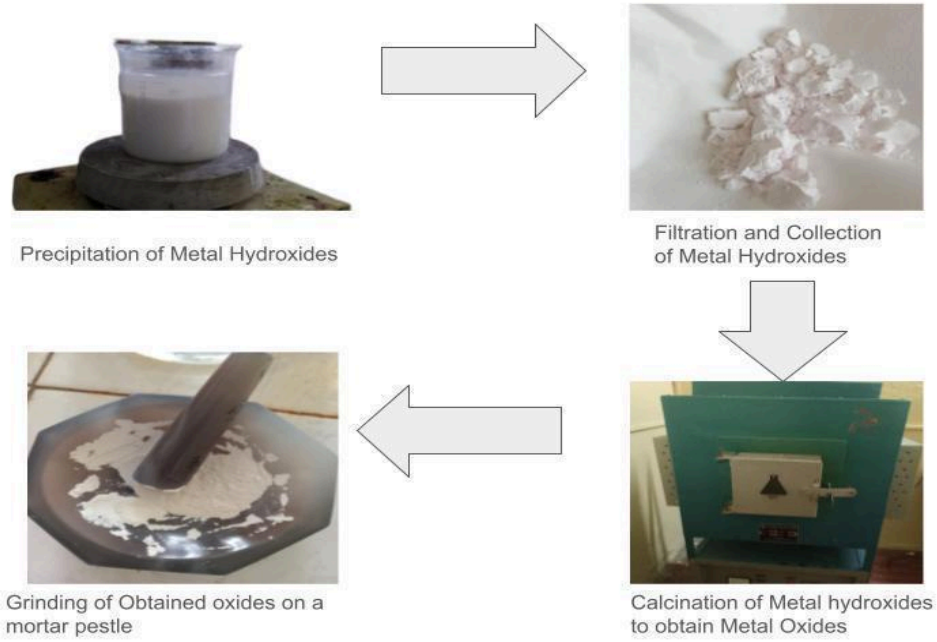

Fig 1: Nanoparticle synthesis procedure (a) Coprecipitation of ZnO nanoparticles, (b) muffle furnace where the hydroxide precipitates were heated, (c) Grinding of the Zinc Oxide nanoparticles in mortar pestle to get a fine powder.

The chemical reaction involved in the precipitation of Zinc Hydroxide precipitate $Zn(OH)_2$ is

$$Zn(NO_3)_2(aq) + 2\ NH_4OH(aq) \rightarrow Zn(OH)_2(s) + 2\ NH_4NO_3(aq)$$

The net ionic equation is

$$Zn^{2+}(aq) + 2OH^-(aq) \rightarrow Zn(OH)_2(s)$$

Similarly, after heating the $Zn(OH)_2$ in a muffle furnace, following thermal decomposition happens.

$$Zn(OH)_2(s) + \Delta \rightarrow ZnO(s) + H_2O(g)$$

All prepared nanomaterials were named as mentioned in Table 1.

3.3 Physicochemical characterization

The optical properties of the as-prepared nanomaterials were assessed using Uv-Vis spectrophotometer;The surface morphology/topography was studied using field scanning electron microscopy (FESEM) and crystallinity was studied using X-ray diffraction (XRD).

3.4 Photocatalytic degradation of Methylene Blue

The photocatalytic degradation performance of the synthesized zinc oxide–based materials was evaluated using methylene blue (MB) as the model organic pollutant. A 10-ppm methylene blue solution was prepared. 250 mL of the MB solution was taken in a beaker. Subsequently, 100 mg of the photocatalyst was introduced into the MB solution, and the suspension was magnetically stirred in the dark for 30 minutes. The preliminary stirring in the dark was done to establish adsorption–desorption equilibrium between the dye molecules and the catalyst surface. Following equilibration, the reaction mixture was exposed to UV irradiation (254 nm) inside a UV chamber (as shown in fig 2) to initiate photocatalytic degradation. At regular intervals of 15 minutes, aliquots of the reaction mixture were withdrawn and centrifuged at 5000 rpm for 10 minutes to separate the photocatalyst particles. The clear supernatant was analyzed spectroscopically to determine the remaining concentration of MB.

Fig 2: The setup where photocatalytic degradation was carried out.
(The probes supplied the UV light to the dye solution containing the photocatalyst in a dark chamber under constant stirring)

3.4 Antimicrobial Tests

3.4.1. Preparation of microbial culture media

The preparation of liquid broth (LB) involved dissolving 13g of LB powder (purchased from Sisco research laboratories Pvt. Ltd, India) in 1 L of distilled water. At 15psi and at 121°C, the mixture was autoclaved for 25 minutes. The media was cooled down to 40-50 °C. It was then transferred into sterilized 15mL falcon tubes. Each tube was filled with 5 mL of the media. The bacterial seed was added to the prepared medium in individual tubes, and the cultures were incubated for 24 hours.

3.4.2. Preparation of MH media plates preparation

The preparation of Mueller-Hinton Agar (MHA) plate involved dissolving 39g of MH agar powder (Sisco research laboratories Pvt. Ltd, India) in 1L of distilled water. At 15 psi and 121 °C, the mixture was autoclaved for 25 minutes. The media was cooled down to 40-50 °C. It was then transferred into sterilized 90mm petri dishes. Each petri dish contained 25mL of the media.

3.4.3. Antimicrobial assay protocol

In a refrigerator, the prepared media was stored. Proper labeling of the sample names were done and 100 µL of freshly cultured liquid bacterial cells were spread with the help of sterile cotton swabs on the surface of media plates. The wells of 9 mm diameter and 3 mm depth were made on the surface of media plates with the back of a sterilized pipette tip to load samples, standard and negative control. The prepared wells were loaded with 100 µL of sample solution (100 mg/mL concentration dissolved in DMSO). The other wells were then loaded with standard, and negative control (DMSO), respectively. Standard Kanamycin solution (3 mg/mL, 10 µL loaded) was used as a positive control. For anti-fungal standard solution, Itraconazole 20 mg/mL, 10 µL was used. For 24 hours, the media plates were then incubated at 37 °C. Then antimicrobial results were observed after.

3.5 Cytotoxicity Tests

Brine shrimp lethality assay is a very simple and cost effective method.With a small amount of test material, the experiment can be conducted. For a preliminary cytotoxicity assay of materials, it is an important tool which is based on the material's ability to kill a laboratory cultured larva (nauplii).The nauplii get exposed to different concentrations (lowest to highest) of samples for 24 hours. The number of alive nauplii are counted and expressed in percentage mortality to know effectiveness of the samples.

3.5.1 Brine shrimp lethality assay (cytotoxicity) protocol

Brine shrimp were cultured in artificial seawater prepared by dissolving 30 g/L of salt in water. Approximately 100 mg of brine shrimp eggs were inoculated into this solution and incubated at a temperature range of 22–29°C under continuous aeration using an air pump. The eggs hatched into nauplii within 60–72 hours, and these were subsequently used for cytotoxicity assays. For each sample concentration, 20 nauplii were placed in individual wells of a 96-well plate. A 10 mg sample was accurately weighed into a clean E-tube, dissolved in 1 mL of DMSO, and further diluted with 9 mL of distilled water to obtain a stock solution of 1000 ppm. Serial dilutions were then prepared to achieve concentrations of 10, 50, 100, 500, and 800 ppm. Each well, with a capacity of 0.5 mL, was inoculated with 20 nauplii and loaded with 0.4 mL of the respective diluted sample. All samples were tested in triplicate to ensure accuracy. The experiment was monitored closely for 8 hours and continued for a total of 24 hours. Complete mortality of nauplii was observed after 24 hours. A sample was considered cytotoxic if it caused 50% or more mortality among the nauplii. The provided sample was analyzed following this procedure, and the results obtained are presented in the table.

3.6 Radical Scavenging Activity (RSA) - DPPH Assay

The antioxidant activity of the samples ZnO, Ce(0.5)-ZnO, Co(0.5)-ZnO, and CoCe(0.25)-ZnO was evaluated using the DPPH assay. Each sample was dissolved in absolute ethanol to prepare five different concentrations: 10 mg/mL, 8 mg/mL, 6 mg/mL, 4 mg/mL, and 2 mg/mL. For the assay, 1 mL of each sample solution was mixed with 3 mL of 0.2 mM ethanolic DPPH solution, thoroughly mixed, and incubated at 30°C in complete darkness for 30 minutes. A control was prepared by mixing 1 mL of ethanol (without sample) with 3 mL of 0.2 mM DPPH solution

under identical conditions. All tests were performed in triplicates. Ascorbic acid was used as a standard antioxidant, prepared by dissolving 6 mg in 3 mL of absolute methanol, followed by serial dilutions to obtain concentrations of 2 mg/mL, 1 mg/mL, 0.5 mg/mL, 250 µg/mL, and 125 µg/mL. Each standard solution (1 mL) was mixed with 3 mL of DPPH solution and incubated similarly. The DPPH working solution was prepared by dissolving 7.8 mg of DPPH powder in 100 mL of absolute methanol and stored at 4°C. After incubation, the absorbance of all samples and standards was measured at 517 nm against a blank to determine radical scavenging activity. The percentage inhibition (%) of free radical DPPH was calculated as follows:

% radical scavenging activity (RSA) = Abs control – Abs sample /Abs control *100 %

Where: Abs control = Absorbance of the control reaction (DPPH without the test fraction) Abs sample = Absorbance of DPPH incubated with sample concentration.

Chapter 4 - Results and Discussion

4.1 Physicochemical Characterization

4.1.1 UV-Vis Spectroscopy

The UV–Vis absorption spectra of ZnO, Ce-doped ZnO, Co-doped ZnO, and Co–Ce co-doped ZnO showed the characteristic near-UV absorption edge associated with the intrinsic bandgap of ZnO nanoparticles. All samples showed strong absorption between 350–400 nm, consistent with a direct bandgap semiconductor. Doping with Ce and co-doping with Ce and Co produced a slight redshift in the absorption edge, while Co doping alone resulted in a marginal blue-shift, indicating subtle modifications of the electronic band structure due to dopant incorporation.

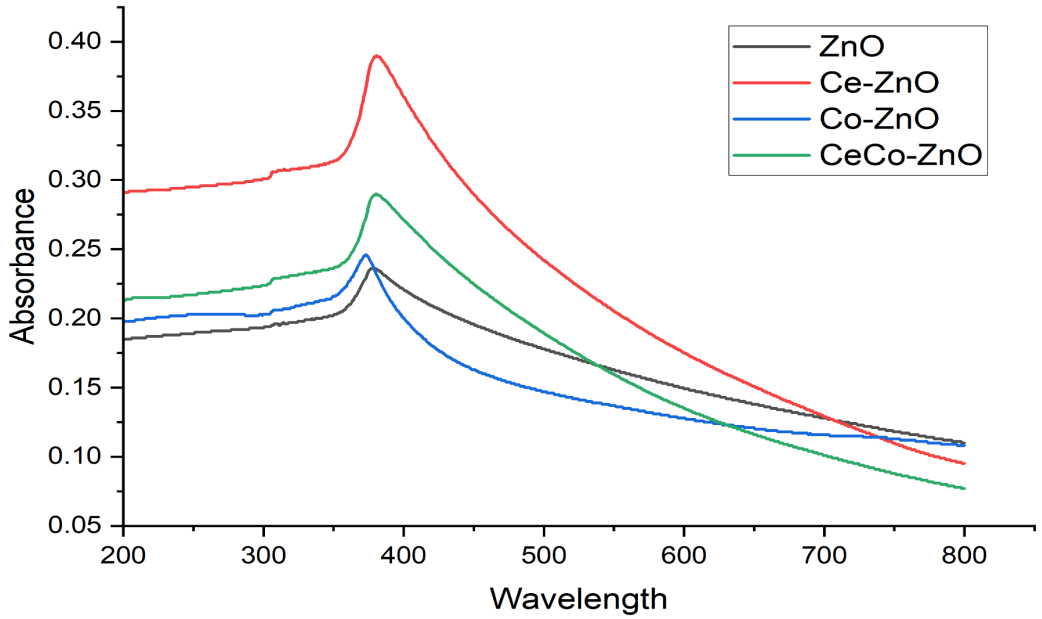

Fig 3: Uv- Vis plots of various samples: ZnO, Ce-doped ZnO, Co-doped ZnO, Ce-Co co-doped ZnO

4.1.2 XRD

The XRD patterns of the samples show main peaks at around 31.7°, 34.4°, 36.2°, 47.5°, 56.5°, 62.8°, and 67.9° (2θ), which match the hexagonal wurtzite structure of ZnO. These peaks belong to planes (100), (002), (101), (102), (110), (103), and (112). This confirms that ZnO is the major phase in all samples. Samples have sharp peaks without extra reflections, which means it is pure ZnO with good crystallinity. Doping changes the structure of ZnO in different ways. When dopant ions replace Zn ions, the lattice size changes and peaks can shift slightly. Peak broadening is also seen in doped samples, which means smaller crystallite size and more strain in the lattice. This happens because dopant ions have different sizes than Zn ions, so they create distortion.

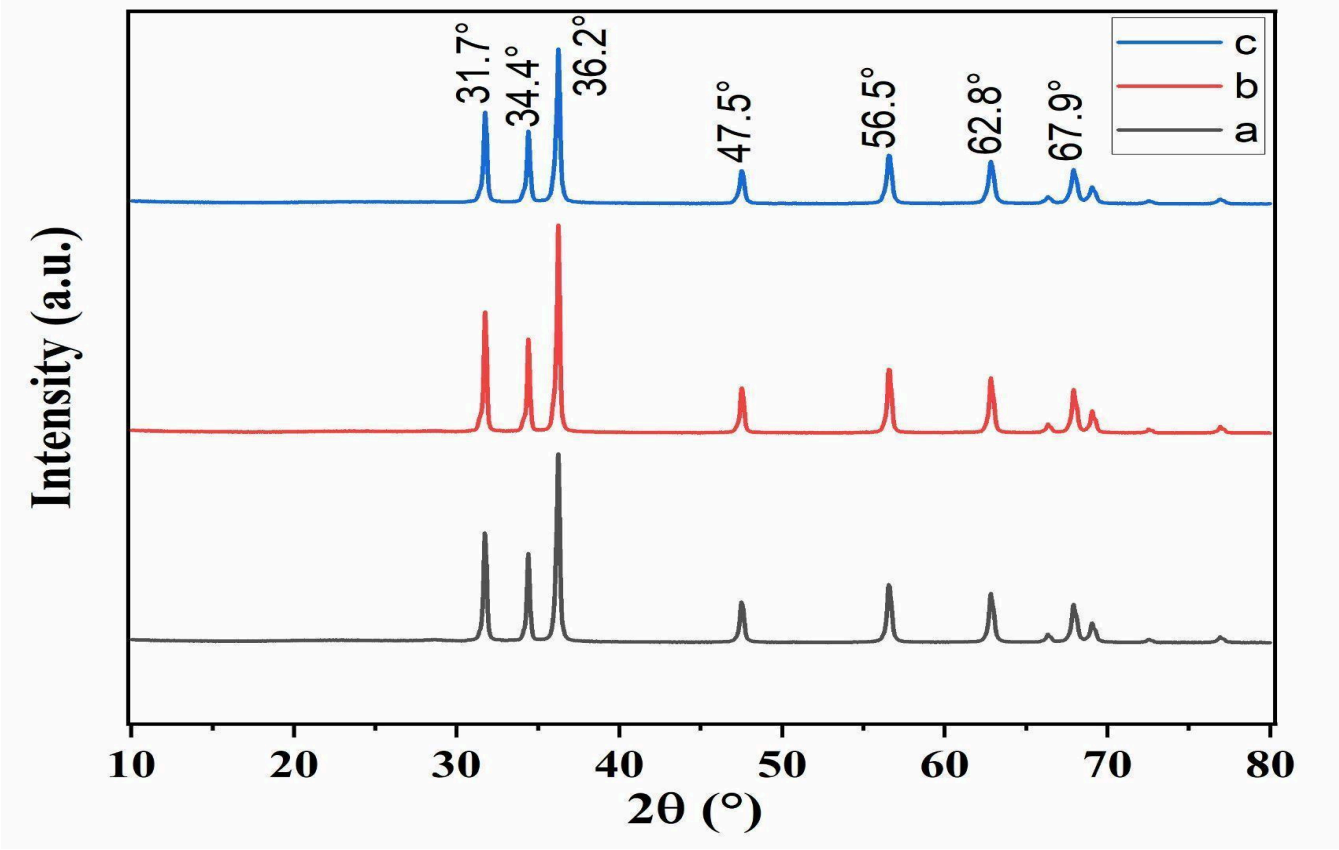

Fig 4: XRD analysis curve of ZnO NP samples at 2θ°.

4.1.3 FESEM

ZnO NPs and their doped counterparts' surface morphology were examined using FE-SEM. The obtained images are presented in fig.1. In undoped Zinc Oxide, irregular, quasi-spherical morphology was observed. A noticeable agglomeration was observed. A broad particle size distribution ranging from approximately 80 to 120 nm was observed in the image. The particles appeared loosely packed with distinct intergranular voids.

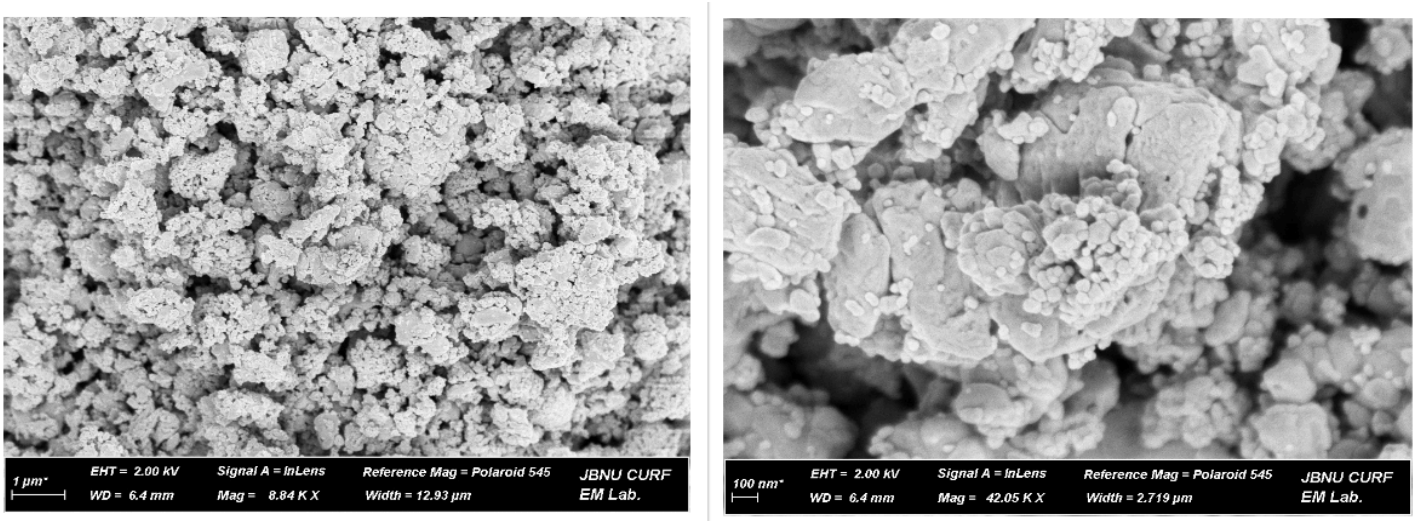

Fig 5: FESEM images of undoped ZnO nanoparticles.

Doping with Cerium made the surface more compact and homogenous with smoother surfaces and smaller particle sizes of around 60-90 nanometers. This change in morphology suggests that Ce incorporation had an important impact on the grain growth which altered the particle aggregation leading to improved uniformity in the nanostructure.

Fig 6 : FESEM images of Ce(0.5)-ZnO NPs

Relatively fine-grained particles with moderate porosity and slightly rough surfaces compared to Ce-doped ZnO were observed with Co-doped ZnO. The images indicated the formation of smaller crystallites of 70-100 nm. It showed a potential improvement in surface area.

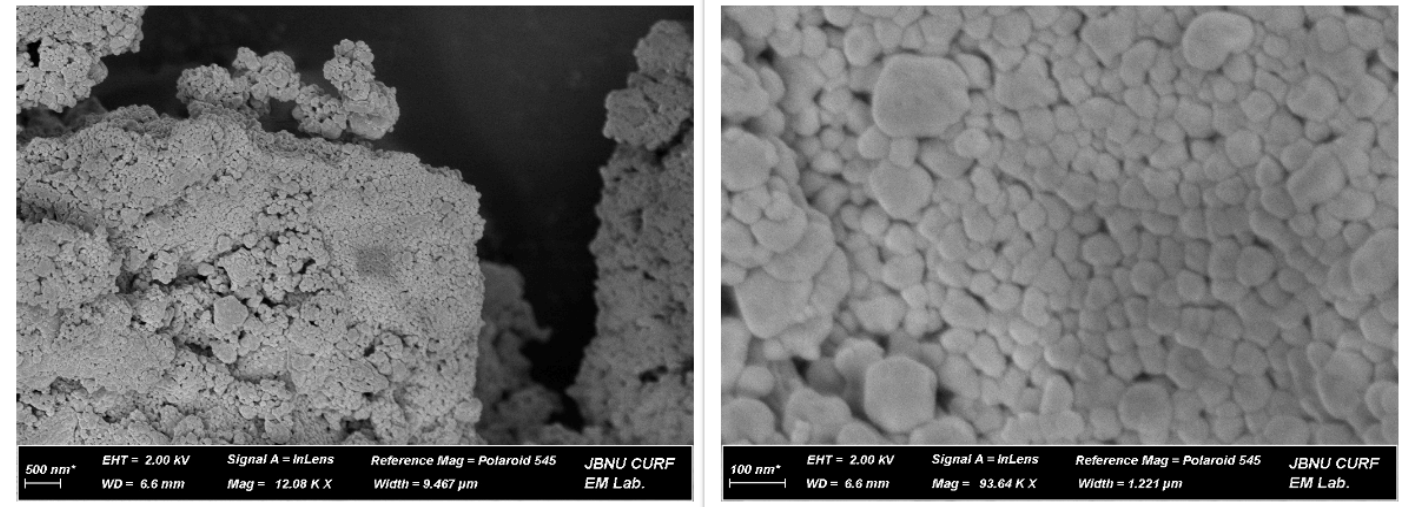

Fig 7: FESEM images of Co(0.5)-ZnO NPs

The Ce-Co co-doped ZnO showed the most uniform and densely packed nanostructure with particles in the range of 50-80 nm. The codoping effect seems to have synergistically regulated the nucleation and growth process, producing a more refined and stable structure. The FESEM

analysis has confirmed that doping with Ce and Co significantly modified the ZnO's structure, reducing particle size, improving uniformity and increasing surface compactness.

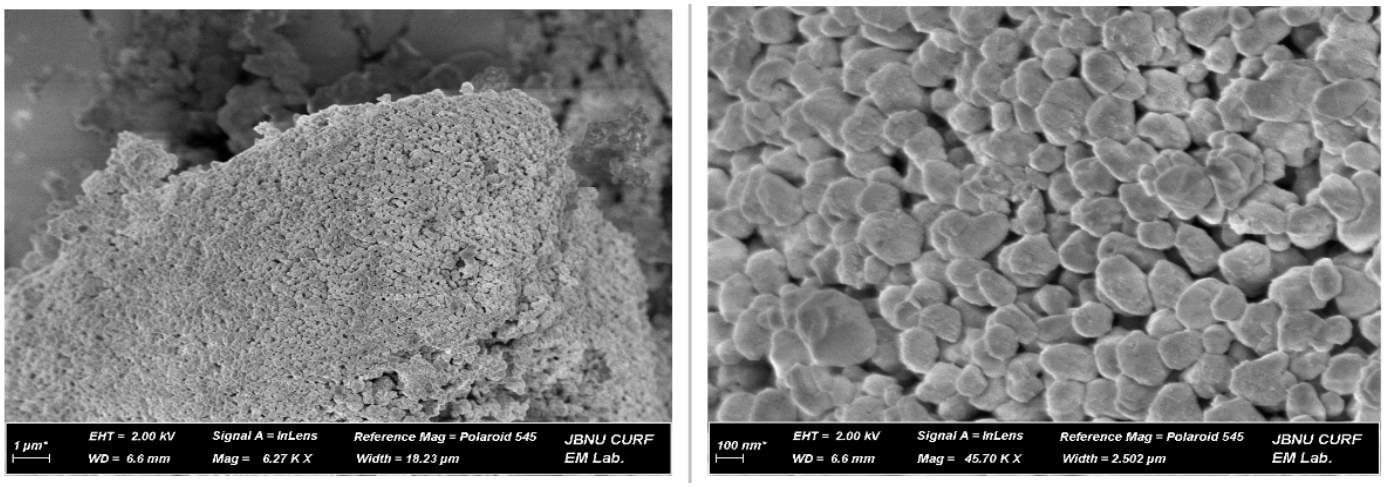

Fig 8: FESEM images of CoCe(0.25)-ZnO NPs.

4.1.4 EDS

The elemental analysis through EDS on the co-doped sample (CoCe(0.25)-ZnO) revealed that Zinc and Oxygen were the predominant compounds with minor traces of Cobalt and Cerium. The quantitative data of Zn constituting 74.23 wt% and O constituting 22.69% suggested that the material's primary phase is Zinc Oxide. This inference is further supported by close correspondence of atomic percentages of Zinc (45.06%) and Oxygen (54.63%). Detection of small amounts of Co(0.2 wt%) and Ce(0.63 wt%) shows the intention of doping being successful.

Table 2 : Constituent Elements Obtained from EDS

Element	Apparent Concentration	Wt%	At%
Oxygen	33.55	22.69	54.63
Cobalt	0.28	0.20	0.13
Zinc	74.23	76.48	45.06
Cerium	0.79	0.63	0.17
Total	100	100	100

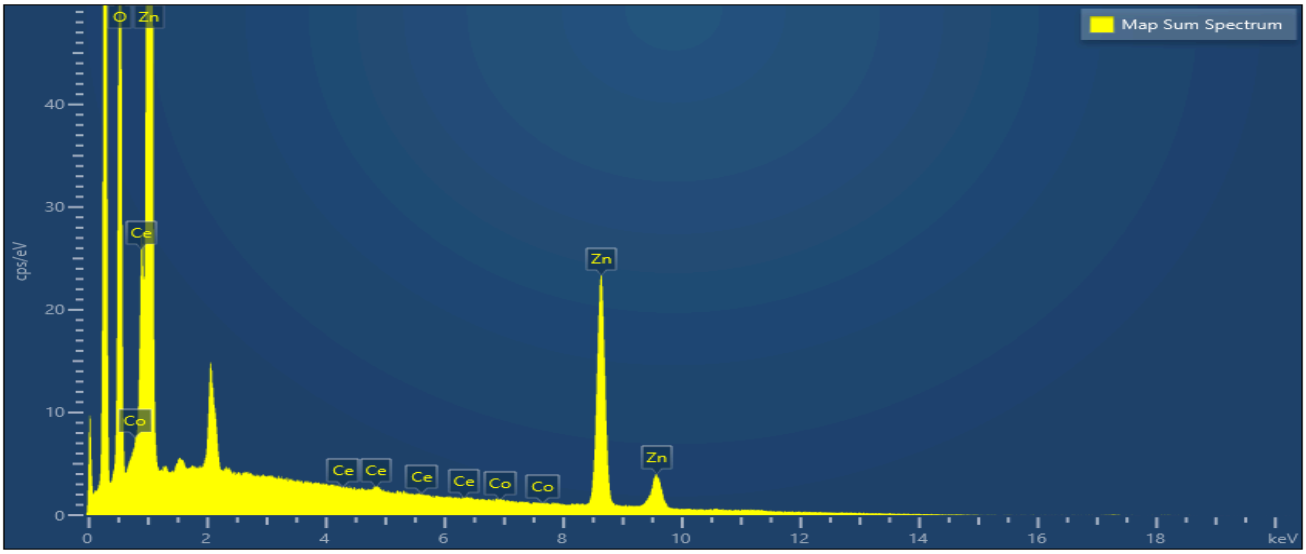

Fig 9: EDS Curve of Ce-Co co-doped ZnO NPs

The distribution of constituent elements across the particles were observed with elemental mapping images. It showed a uniform distribution of dopant atoms across the host atoms.

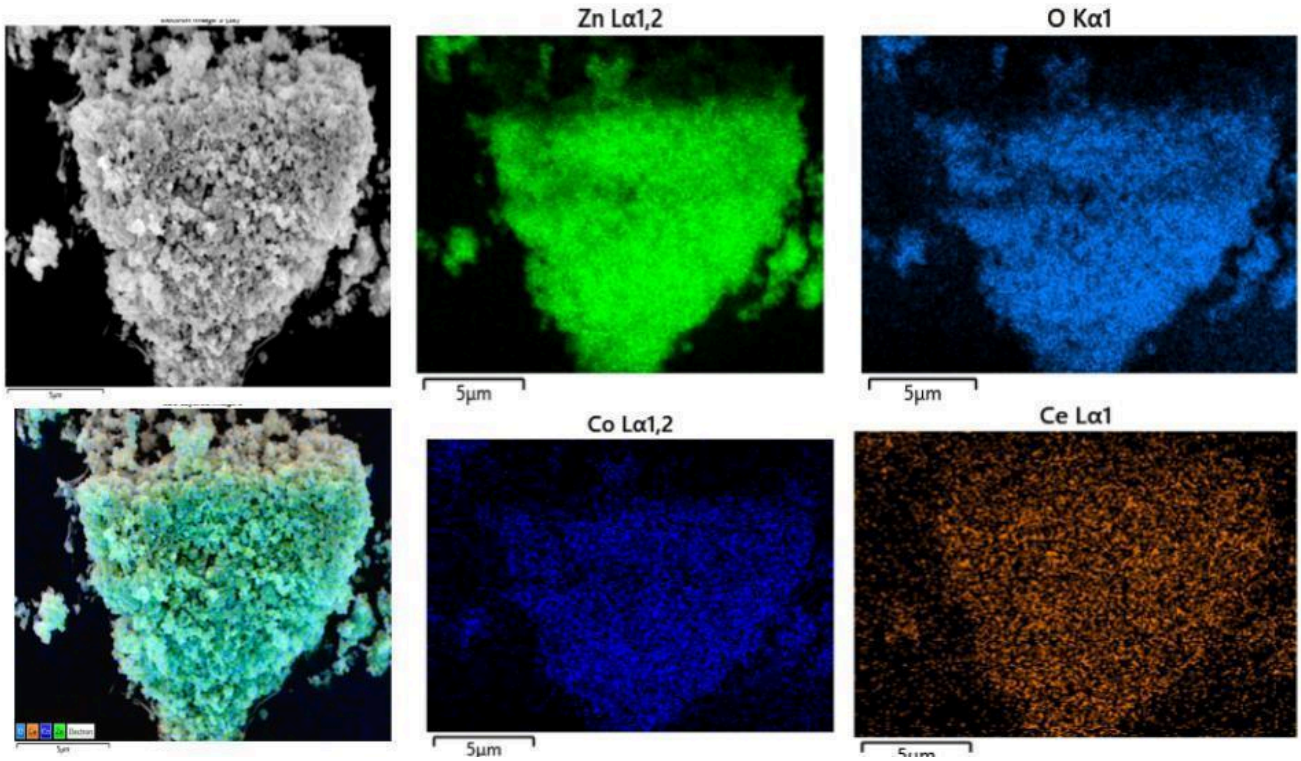

Fig 10 : Distribution of various elements across the particle of (CoCe(0.25)-ZnO)

4.2 Assessment of Dye-degradation and Antimicrobial Properties

4.2.1 Photocatalytic Degradation of Methylene Blue

The degradation of Methylene blue was visually observable. With the passage of time, there was a gradual reduction in color of the dye which was visually distinguishable. By the end of the 2 hours of photocatalytic process, the dye appeared almost as clear as distilled water.

Fig 11 : Visual Observation of gradual degradation of MB in CoCe(3)-ZnO

For methylene blue (MB), the characteristic peak is around 664 nm. The absorbance values obtained from UV-Vis spectroscopy for each of the samples are tabulated in Table 4

Table 3: Absorbance of Methylene blue across various time intervals

Time (min)	ZnO	Ce(0.5)-ZnO	Ce(1)-ZnO	Ce(3)-ZnO	CoCe(0.5)-ZnO	CoCe(1)-ZnO	CoCe(3)-ZnO
Initial Solution	1.977	1.977	1.952	1.917	1.611	1.875	1.581
After 30 mins of stirring in dark	1.793	1.941	1.894	1.896	1.500	1.947	1.535
15 mins	1.146	1.262	1.173	1.756	0.984	1.158	1.175
30 mins	0.762	0.759	0.832	1.564	0.608	0.655	0.922
45 mins	0.548	0.445	0.537	1.420	0.445	0.349	0.468
60 mins	0.369	0.226	0.304	1.050	0.264	0.161	0.196

75 mins	0.247	0.116	0.162	0.807	0.149	0.093	0.076
90 mins	0.144	0.063	0.090	0.590	0.082	0.041	0.047
105 mins	0.082	0.033	0.064	0.397	0.036	0.029	0.019
120 mins	0.056	0.015	0.080	0.269	0.018	0.004	0.015

With these absorbance values, the degradation ratios for each of the samples were calculated using the formula

$$\text{Degradation Ratio} = (A_0 - A_t)/A_0 \text{ where,}$$

A0 = initial absorbance

At = absorbance at time t

Now based on this absorbance, the degradation ratios were calculated for each of the samples and tabulated in Table 5.

Table 4: Degradation ratios of Methylene Blue using various nanoparticles

Time (min)	ZnO	Ce(0.5)-ZnO	Ce(1)-ZnO	Ce(3)-ZnO	CoCe(0.5)-ZnO	CoCe(1)-ZnO	CoCe(3)-ZnO
0	0.0931	0.0182	0.0297	0.0110	0.0689	-0.0384	0.0291
15	0.4203	0.3617	0.3991	0.0840	0.3892	0.3824	0.2568
30	0.6146	0.6161	0.5738	0.1841	0.6226	0.6507	0.4168
45	0.7228	0.7749	0.7249	0.2593	0.7238	0.8139	0.7040
60	0.8134	0.8857	0.8443	0.4523	0.8361	0.9141	0.8760
75	0.8751	0.9413	0.9170	0.5790	0.9075	0.9504	0.9519
90	0.9272	0.9681	0.9539	0.6922	0.9491	0.9781	0.9703
105	0.9585	0.9833	0.9672	0.7929	0.9777	0.9845	0.9880
120	0.9717	**0.9924**	0.9590	0.8597	0.9888	**0.9979**	**0.9905**

The absorbance values around 664 nm, which is the main peak of methylene blue (MB), kept decreasing with time for all the samples. This showed that every sample had some photocatalytic activity. Pure ZnO showed a slow but steady drop in absorbance and reached about 97% degradation after 120 minutes. This is because ZnO naturally works well under UV light, even though its performance is limited by fast electron–hole recombination.

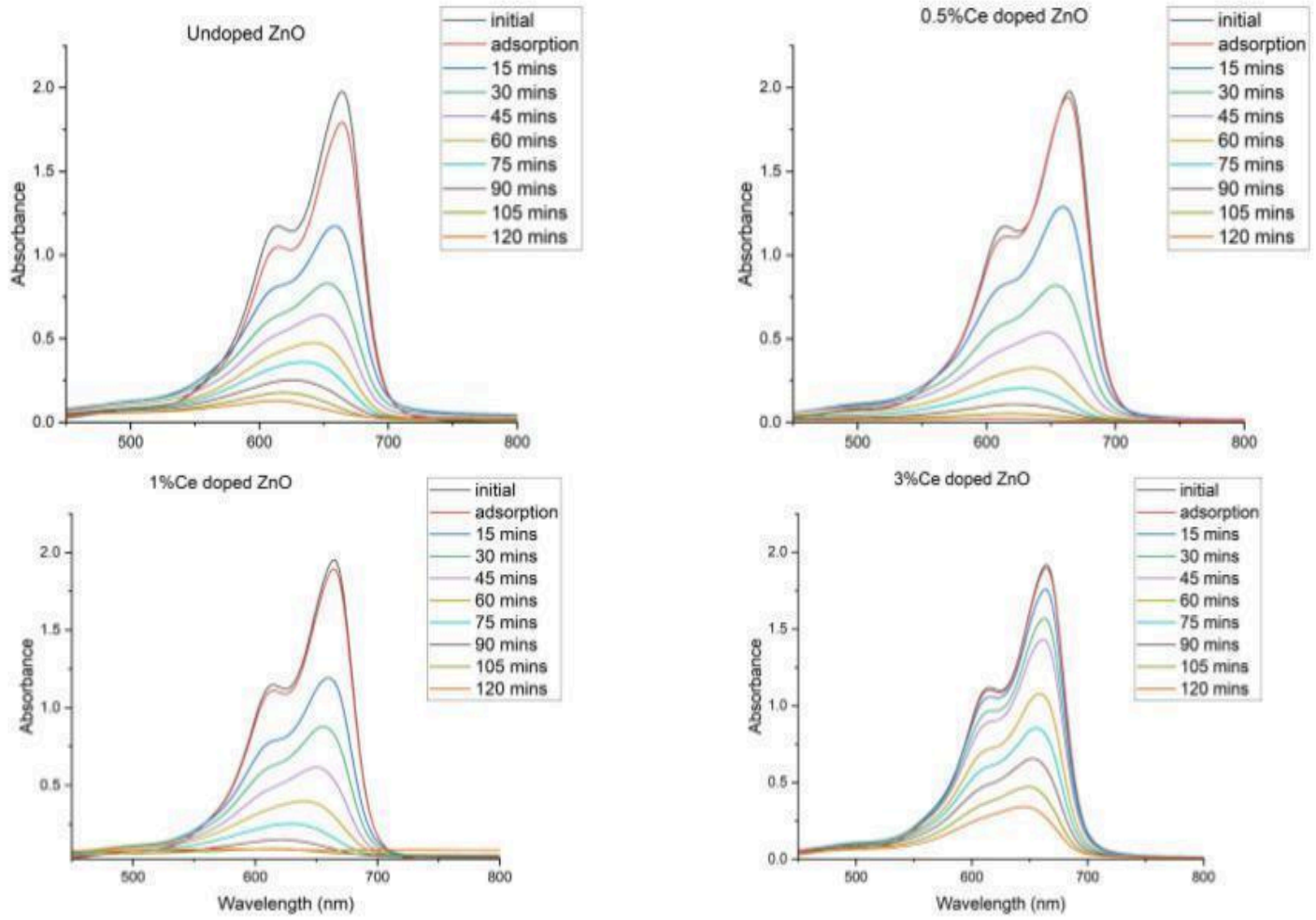

Fig 12: Photocatalytic degradation curve of MB as shown by (a) ZnO, (b)Ce(0.5)-ZnO, (c) Ce(1)-ZnO and (d) Ce(3)-ZnO

When a small amount of cerium (Ce) was added to ZnO, the degradation became much better. The samples with 0.5% and 1% Ce removed 99.2% and 95.9% of the dye in 120 minutes. This happened because Ce^{3+}/Ce^{4+} helps in trapping charges, so recombination becomes slower. But when too much Ce (3%) was added, the performance dropped to 86%, probably because too

many defects formed and blocked charge movement. Doping with cobalt (Co) and using both Co and Ce together improved the photocatalytic activity even more. The sample CoCe(0.5) degraded 98.8% of the dye, and the CoCe(3)-ZnO sample's degradation reached 99.05%. This improvement is mainly because Co helps absorb more UV light, and Ce improves charge separation. The best result came from the CoCe(1)-ZnO sample, which almost completely degraded the dye (99.8%) in 120 minutes. This happened because Co created extra states in the band gap for better light absorption, and Ce acted as an electron trap to reduce recombination. Together, they created a good balance that made the photocatalytic reaction much faster. Overall, the results show that using the right amount of both dopants is important for getting the highest photocatalytic activity in ZnO.

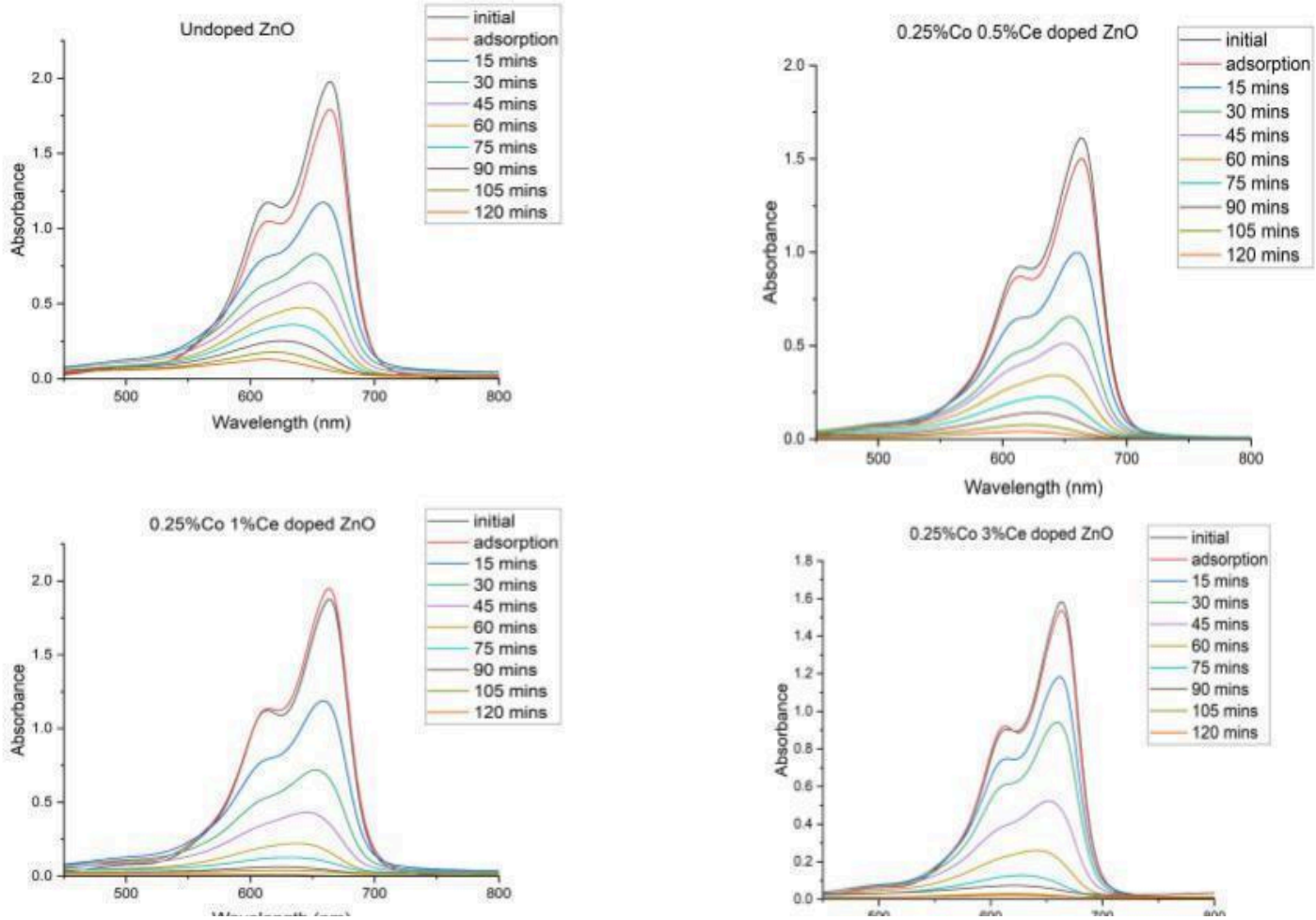

Fig 13: Photocatalytic degradation curve of MB as shown by (a) ZnO, (b)CoCe(0.5)-ZnO, (c) CoCe(1)-ZnO and (d) CoCe(3)-ZnO

4.2.2 Antimicrobial and antifungal activity

The antimicrobial results observed for gram positive and gram-negative bacteria and fungus and tabulated in Table-5. The ZOI has been measured in cm and has been mentioned in the result table. Kanamycin antibiotic in the concentration of 3 mg/mL has been used as positive control (c+) for antibacterial and for antifungal, Itraconazole 20 mg/mL has been used. Negative control didn't show any activity, hence has not been included in the table.

Table 5: Antifungal and antibacterial activity of the prepared ZnO NPs.

Sample Type	*E.coli*	*S. aureus*	*C. albicans*
Positive Control	1.8	2.0	1.7
ZnO	1.2	1.5	1.2
Ce(0.5)-ZnO	1.4	1.4	1.1
Ce(1)-ZnO	1.2	1.3	1.3
Ce(3)-ZnO	1.3	1.7	1.7
Ce(5)-ZnO	1.3	1.5	1.5
CoCe(0.25)-ZnO	1.7	1.6	1.4
CoCe(0.5)-ZnO	1.2	1.6	1.5
CoCe(1)-ZnO	1.1	1.3	1.5
CoCe(3)-ZnO	1.4	1.7	1.7

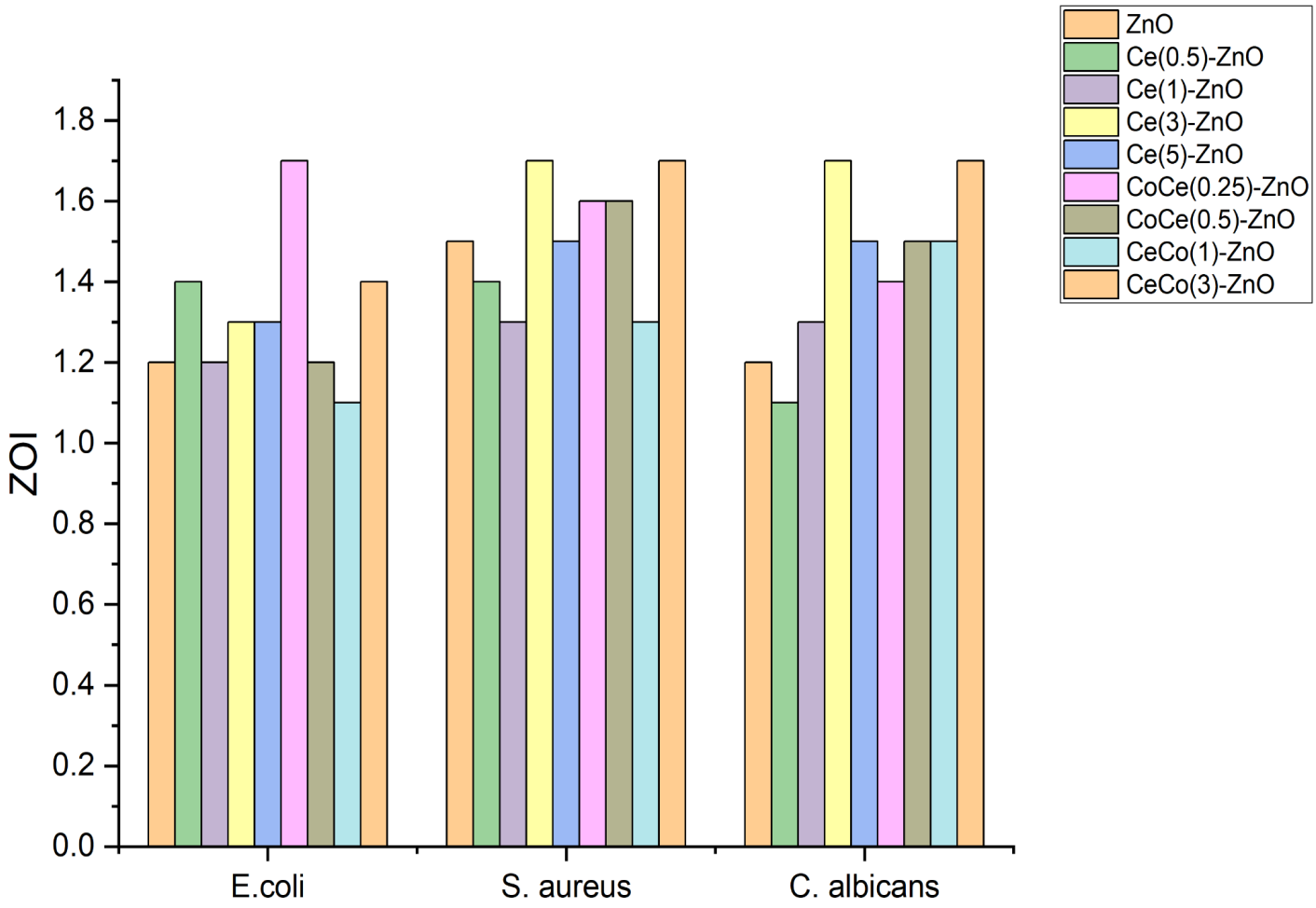

Fig 14 : Antimicrobial performance of prepared nanoparticles for microbes: *E. coli*, *S. aureus*, *C. albicans*

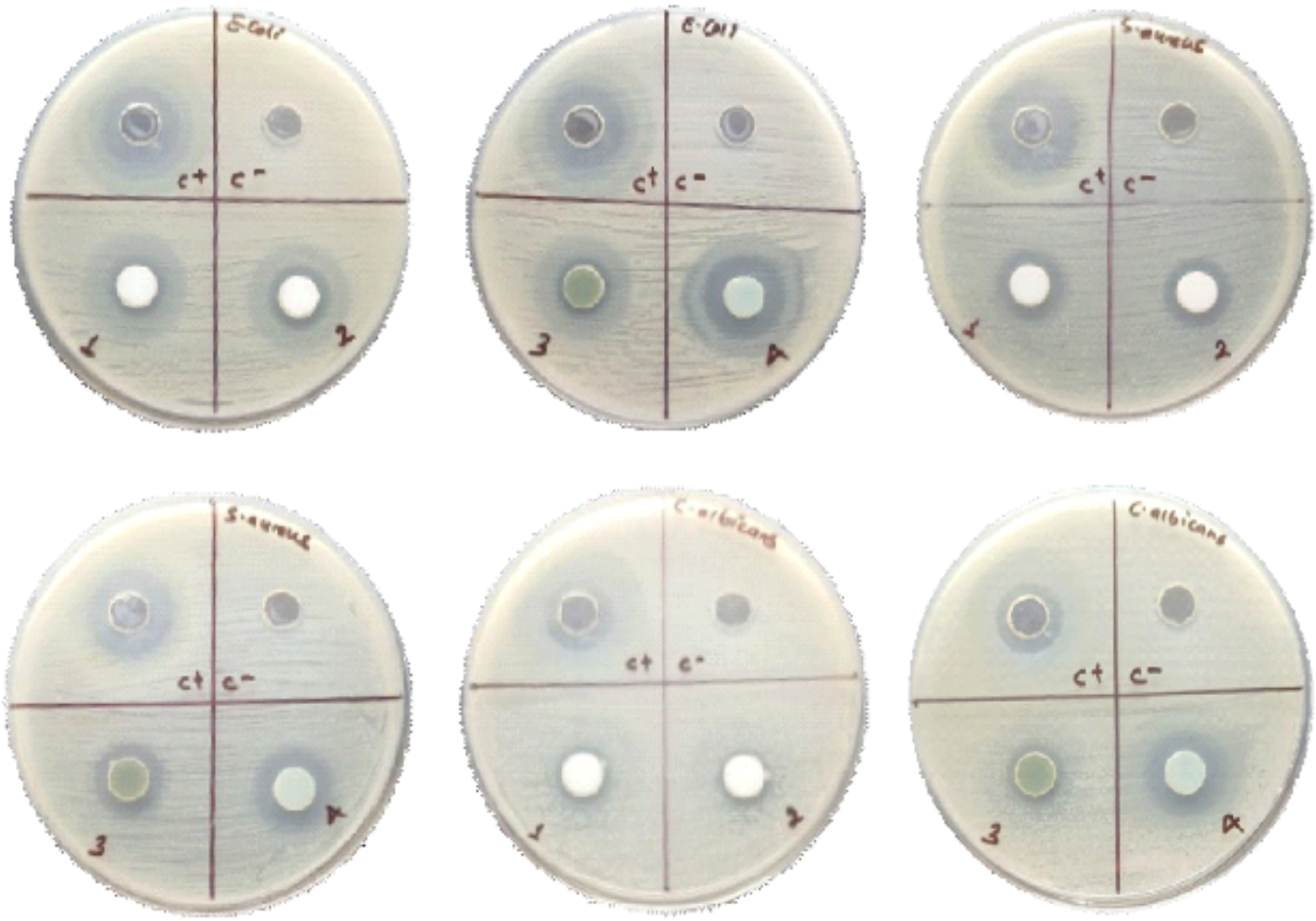

Fig 15 : Antimicrobial test for different sample against different microbes: (a) Test of sample 1 and 2 against *E. coli*, (b) Test of sample 3 and 4 against *E. coli*, (c) Test of sample 1 and 2 against *S. aureus*, (d) Test of sample 1 and 2 against *S. aureus*, (e) Test of sample 1 and 2 against *C. albicans,* (f) Test of sample 3 and 4 against *C. albicans*. Sample 1, 2, 3, and 4 are ZnO NPs, Ce@ZnO NPs, Co@ZnO and CeCo@ ZnO. C^+ is positive control and C^- is negative control. Kanamycin antibiotic in the concentration of 3 mg/mL has been used as positive control (C^+) for antibacterial and for antifungal, Itraconazole 20 mg/mL has been used.

Undoped ZnO showed a moderate ability to stop the growth of all the microorganisms tested, mainly because it can produce reactive oxygen species (ROS) and release Zn^{2+} ions. When Ce was added, the antibacterial activity changed quite a lot. At low Ce levels (0.5–1%), the results were almost the same as pure ZnO or sometimes even a bit lower, which means that a small amount of Ce does not improve the antimicrobial effect much. But when 3% Ce was used, the activity became much stronger, especially against *S. aureus* and *C. albicans*, giving inhibition

zones of about 1.7 cm, similar to the positive control. This increase is probably because the Ce^{3+}/Ce^{4+} redox pair helps produce more ROS and reduces recombination. When Ce was increased to 5%, there was no extra improvement; in some cases, the activity even got worse, likely because too much doping creates defects that act as recombination centers instead of helping.

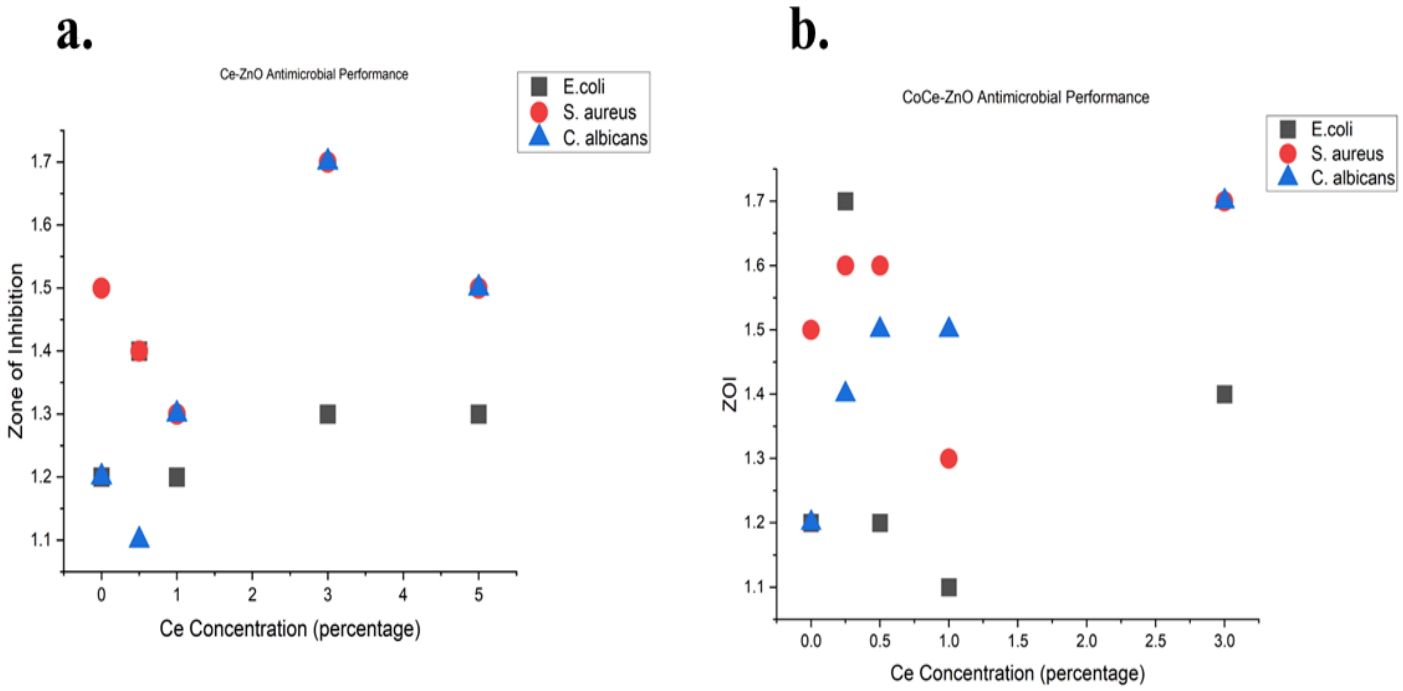

Fig 16 : Variation in antimicrobial activity of ZnO (a) based on doping percentage of Ce (b) based on doping percentage of Ce with fixed 0.25% Co

The Ce–Co co-doped samples showed a different pattern. The sample CoCe(0.25)-ZnO had some of the strongest antimicrobial effects, with a 1.7 cm inhibition zone against *E. coli* and strong activity against *S. aureus* and *C. albicans*. This suggests that Ce and Co work well together: Co^{2+} increases oxygen vacancies and improves charge separation, while Ce helps with redox reactions. But when Ce was increased to medium levels (0.5–1% with the same Co amount), the activity dropped, especially against *E. coli*, showing that the balance between Ce and Co is very important. At a higher Ce amount (CoCe(3)-ZnO), the co-doped sample again showed strong antibacterial and antifungal activity, similar to the best Ce-only sample. In general, the samples worked better against *S. aureus* than *E. coli*, because Gram-negative bacteria like *E. coli* are naturally more resistant due to their complex outer membrane. The

antifungal activity followed a similar trend, with doped samples especially those with 3% Ce showing inhibition close to the positive control. Overall, the results showed that using the right doping amount, especially 3% Ce or certain Ce–Co combinations, can greatly improve the antimicrobial activity of ZnO by increasing ROS production, creating more oxygen vacancies, and improving charge separation, which together make it easier to damage microbial cells.

4.2.3 Cytotoxicity results of the prepared samples on Nauplii

Toxicity across various samples were revealed with brine shrimp lethality assay.The mortality rate steadily increased from 0 to 1000 ppm for over 24 hours. Based on pooled triplicate counts (n = 60 nauplii per dose) and LC_{50} estimation via log-scale interpolation between doses surrounding 50% mortality, the co-doped CoCe(0.25)-ZnO sample showed the highest toxicity, CoCe(0.25) had an LC_{50} of approximately 100 ppm. Pure ZnO displayed moderate toxicity with its observed 43.3% mortality at 100 ppm and 60.0% at 500 ppm. Co(0.5)ZnO behaved similarly with 41.7% mortality at 100 ppm, 60.0% at 500 ppm, and full lethality at 1000 ppm. Conversely, Ce(0.5)ZnO was least toxic, 46.7% at 500 ppm, 58.3% at 800 ppm, and 88.3% at 1000 ppm). Overall, the 24-hour acute toxicity ranking is CoCe(0.25)ZnO > ZnO ≈ Co(0.5)ZnO > Ce(0.5)ZnO, indicating that cobalt–cerium co-doping enhances toxicity synergistically compared to pure ZnO or single-dopant variants, while cerium alone reduces toxicity.

Table 6 :Brine shrimp lethality assay of Cerium and Cobalt Codoped Zinc Oxide.

Sample	Concentration (ppm)	Number of alive nauplii after 24 hours in each replication			Mortality (%)	Remarks
		T1	T2	T3		
ZnO	0	20	20	20	0	Nauplii started dying at the concentration of 50 ppm. 50% (or
	10	20	20	20	0	
	50	15	17	14	23	
	100	12	13	9	43	
	500	9	9	6	60	
	800	5	4	3	80	

	1000	0	0	0	100	more) of the tested nauplii died at the highest concentration of 500 ppm. Hence, LC50 of sample 1 is at 500 ppm (500 µg/mL)
Ce(0.5)-ZnO	0	20	20	20	0	Nauplii started dying at the concentration of 50 ppm. 50% (or more) of the tested nauplii died at the highest concentration of 800 ppm. Hence, LC50 of sample 2 is at 800 ppm (800 µg/mL)
	10	20	20	20	0	
	50	17	16	17	16	
	100	14	13	13	33	
	500	11	10	11	46	
	800	9	8	8	58	
	1000	3	2	2	88	

Co(0.5)-ZnO	0	20	20	20	0	Nauplii started dying at the concentration of 10 ppm. 50% (or more) of the tested nauplii died at the highest concentration of 500 ppm. Hence, LC50 of sample 3 is at 500 ppm (500 µg/mL)
	10	18	19	18	8	
	50	15	16	14	25	
	100	11	12	12	41	
	500	8	9	7	60	
	800	3	3	2	86	
	1000	0	0	0	100	
CoCe(0.25)-ZnO	0	20	20	20	0	Nauplii started dying at the concentration of 10 ppm. 50% (or more) of the tested nauplii died at the highest concentra
	10	15	14	14	28	
	50	10	12	11	45	
	100	8	10	10	53	
	500	5	5	4	76	
	800	0	0	0	100	
	1000	0	0	0	100	

						tion of 100 ppm. Hence, LC50 of sample 4 is at 100 ppm (100 µg/mL)

4.3 Radical Scavenging Activity (RSA)

The DPPH radical-scavenging assay validated the method via the ascorbic acid positive control, which showed clear, concentration-dependent antioxidant activity: mean absorbance fell from 1.013 at 0.125 mg/mL to 0.289 at 2 mg/mL, corresponding to an increase in % inhibition from 66.24% to 90.38%, confirming robust RSA under the assay conditions.

Table 7: Radical scavenging activity of ascorbic acid

Ascorbic acid	concentration mg/mL	Abs 1	Abs 2	Abs 3	Abs mean	% inhibition
1	Control	3	3	3	3	0
2	0.125	1.011	1.015	1.012	1.013	66.24
3	0.25	0.889	0.87	0.869	0.876	70.8
4	0.5	0.669	0.67	0.66	0.666	77.79
5	1	0.421	0.425	0.441	0.429	85.7
6	2	0.291	0.295	0.28	0.289	90.38

In contrast, all four nanomaterial samples ZnO, Ce(0.5)-ZnO Co(0.5)-ZnO, and CoCe(0.25)ZnO exhibited no measurable RSA across the tested range (2–10 mg/mL), with Abs mean = 3.0 at every concentration (identical to the control) and % inhibition = 0% throughout, indicating negligible radical-quenching capacity under these conditions. Consistently, a lack of visible color change upon reaction with DPPH was noted for all samples, further supporting the conclusion that these materials did not scavenge DPPH radicals within the examined dose window. The obtained data have been tabulated and % RSA activities of each concentration have been tabulated in Table 8.

Table 8: RSA activities of ZnO samples

Sample	Concentration (mg/mL)	Abs 1	Abs 2	Abs 3	Abs mean	% inhibition
ZnO	Control (0 mg/mL)	3	3	3	3	0
	2	3	3	3	3	0
	4	3	3	3	3	0
	6	3	3	3	3	0
	8	3	3	3	3	0
	10	3	3	3	3	0
Ce(0.5)-ZnO	Control (0 mg/mL)	3	3	3	3	0
	2	3	3	3	3	0
	4	3	3	3	3	0
	6	3	3	3	3	0
	8	3	3	3	3	0
	10	3	3	3	3	0
Co(0.5)-ZnO	Control (0 mg/mL)	3	3	3	3	0
	2	3	3	3	3	0
	4	3	3	3	3	0
	6	3	3	3	3	0
	8	3	3	3	3	0

	10	3	3	3	3	0
CoCe(0.25)-ZnO	Control (0 mg/mL)	3	3	3	3	0
	2	3	3	3	3	0
	4	3	3	3	3	0
	6	3	3	3	3	0
	8	3	3	3	3	0
	10	3	3	3	3	0

No colour change was observed during reaction with the DPPH solution with all of the tested samples. Hence no radical scavenging activities were observed in all the tested samples.

The results of this study show clearly that adding cerium and cobalt into the ZnO structure changes both the shape and the behavior properties of the nanomaterials. The FESEM images showed that when ZnO was doped, the particles became smaller and the surface looked more even, which means the dopant ions affected how the particles formed during synthesis. These changes in shape, along with small shifts seen in the UV–Vis absorption, suggest that new defect states were created and the band structure was changed in a way that could affect how charges move inside the material. The improvements seen in the photocatalytic breakdown of methylene blue match this idea. Both Ce-doped and Co-doped samples worked better than pure ZnO, and the co-doped samples worked the best. This is likely because doping creates more oxygen vacancies and charge-trapping sites, which help stop electron–hole recombination and make redox reactions happen faster. The effects also depended on the dopant amount, especially in Ce-doped samples, showing that too much dopant can reduce photocatalytic activity instead of improving it.

A similar trend appeared in the antimicrobial and antifungal tests. All ZnO samples showed some microbial inhibition, but the doped ones produced larger inhibition zones, with some Ce–Co combinations showing the strongest results. *S. aureus* was easier to kill than *E. coli*,

which makes sense because Gram-negative bacteria like *E. coli* have an extra outer membrane that protects them from ROS and metal-ion damage. The strong performance of the co-doped samples suggests that the same features that improved photocatalysis like oxygen vacancies and increased surface reactivity also helped damage microbial cell membranes. Overall, the results show that co-doping ZnO with Ce and Co is an effective way to adjust its physical and chemical properties. By choosing the right dopant amounts, it is possible to improve both photocatalytic and antimicrobial activity at the same time, making co-doped ZnO a useful multifunctional material for environmental and biological applications where controlled redox reactions and surface activity are important.

Chapter 5 - Conclusions

Zinc oxide nanoparticles were successfully prepared by coprecipitation method. Cerium and cobalt were doped onto zinc oxide nanoparticles. In addition, cerium and cobalt were codoped onto the zinc oxide nanoparticles. This study successfully synthesized pure, Ce-doped, Co-doped, and Ce–Co co-doped ZnO nanoparticles using a chemical co-precipitation route followed by calcination. Comprehensive physicochemical analyses confirmed effective dopant incorporation, bandgap tuning, and improved morphological uniformity, particularly in the co-doped samples. The Ce–Co co-doped ZnO demonstrated the most notable enhancements, exhibiting a reduced bandgap, finer particle distribution, and superior functional performance. Photocatalytic experiments showed that the 0.25% Co + 1% Ce co-doped ZnO achieved exceptional methylene blue degradation (~99.8% within 120 minutes), while antimicrobial assays revealed significantly larger inhibition zones—up to 17 mm—against E. coli, S. aureus, and C. albicans. Overall, the results highlight Ce–Co co-doping as a promising strategy to enhance the multifunctional capabilities of ZnO nanoparticles, making them strong candidates for advanced environmental remediation and biomedical applications.

1.5 Limitations of the study

The photocatalytic performance was evaluated only under UV light using methylene blue as the representative dye, which does not fully represent real wastewater conditions containing diverse contaminants, varying pH levels, and wide categories of dyes. Similarly, antimicrobial activity was tested against selected bacterial and fungal strains under controlled laboratory conditions, which may not reflect complex clinical and environmental scenarios. Furthermore, the investigation focused on a fixed percentage concentration (0.25% atomic percentage) of Co and variation was done for Ce only.

References

Ahmad, T., Wani, I. A., Lone, I. H., Ganguly, A., Manzoor, N., Ahmad, A., ... & Al-Shihri, A. S. (2013). Antifungal activity of gold nanoparticles prepared by solvothermal method. Materials Research Bulletin, 48(1), 12-20. https://doi.org/10.1016/j.materresbull.2012.09.069

Al Bitar, M., Hassanieh, B., Awad, R., & Khalil, M. (2023). Characterization and evaluation of the therapeutic benefits of pure and lanthanides mono- and co-doped zinc oxide nanoparticles. *Saudi Journal of Biological Sciences, 30*(3), 103608. https://doi.org/10.1016/j.sjbs.2023.103608

Bharat, T. C., Shubham, S., Mondal, S., Gupta, H. S., Singh, P. K., & Das, A. K. (2019). `Synthesis of doped zinc oxide nanoparticles: A review. *Materials Today: Proceedings, 11*, 767–775. https://doi.org/10.1016/j.matpr.2019.03.041

Chen, X., Lou, Y., Dayal, S., Qiu, X., Krolicki, R., Burda, C., Zhao, C., & Becker, J. (2005). Doped semiconductor nanomaterials. *Journal of Nanoscience and Nanotechnology, 5*(9), 1408–1420. https://doi.org/10.1166/jnn.2005.310

Das, S., Mitra, S., Khurana, S. M. P., & Debnath, N. (2013). Nanomaterials for biomedical applications. *Frontiers in Life Science, 7*(3–4), 90–98. https://doi.org/10.1080/21553769.2013.869510

Geldasa, F. T., Kebede, M. A., Shura, M. W., & Gashaw, F. (2023). Experimental and computational study of metal oxide nanoparticles for the photocatalytic degradation of organic pollutants: A review. *RSC Advances, 13*, 18404–18442. https://doi.org/10.1039/d3ra01505j

Hajipour, M. J., Fromm, K. M., Ashkarran, A. A., Jimenez de Aberasturi, D., Ruiz de Larramendi, I., Rojo, T., Serpooshan, V., Parak, W. J., & Mahmoudi, M. (2012). Antibacterial properties of nanoparticles. *Trends in Biotechnology, 30*(10), 499–511. https://doi.org/10.1016/j.tibtech.2012.06.004

Ijaz, M., Zafar, M., Islam, A., Afsheen, S., & Iqbal, T. (2020). A review on antibacterial properties of biologically synthesized zinc oxide nanostructures. *Journal of Inorganic and Organometallic Polymers and Materials, 30*(8), 2819–2831. https://doi.org/10.1007/s10904-020-01603-9

Klefenz, H. (2004). Nanobiotechnology: From molecules to systems. *Engineering in Life Sciences, 4*(3), 211–218. https://doi.org/10.1002/elsc.200402090

Kumar, R., Umar, A., Kumar, G., & Nalwa, H. S. (2017). Antimicrobial properties of ZnO nanomaterials: A review. *Ceramics International, 43*(5), 3940–3961. https://doi.org/10.1016/j.ceramint.2016.12.062

Kumar, M. P., Josephine, G. A. S., Tamilarasan, G., Sivasamy, A., & Sridevi, J. (2018). Rare earth doped semiconductor nanomaterials and its photocatalytic and antimicrobial activities. *Journal of Environmental Chemical Engineering, 6*(4), 3907-3917. https://doi.org/10.1016/j.jece.2018.05.046

Maier, J. (2017). Doping strategies in inorganic and organic materials. Zeitschrift für anorganische und allgemeine Chemie, 643(23), 2083-2087. https://doi.org/10.1002/zaac.201700317

Manikandan, A., Manikandan, E., Meenatchi, B., Vadivel, S., Jaganathan, S. K., Ladchumananandasivam, R., Henini, M., Maaza, M., & Sundeep Aanand, J. (2017). Rare earth element (REE) lanthanum doped zinc oxide (La: ZnO) nanomaterials: Synthesis structural optical and antibacterial studies. *Journal of Alloys and Compounds*, 723, 1155–1161. https://doi.org/10.1016/j.jallcom.2017.06.336

McNeil, S. E. (2005). Nanotechnology for the biologist. *Journal of Leukocyte Biology, 78*(3), 585–594. https://doi.org/10.1189/jlb.0205074

Nasrollahzadeh, M., Sajadi, S. M., Sajjadi, M., & Issaabadi, Z. (2019). An introduction to nanotechnology. In M. Nasrollahzadeh, S. M. Sajadi, M. Sajjadi, & Z. Issaabadi (Eds.), *Interface science and technology* (Vol. 28, pp. 1–27). Elsevier. https://doi.org/10.1016/B978-0-12-813586-0.00001-8

Niemirowicz, K., Durnaś, B., Piktel, E., & Bucki, R. (2017). Development of Antifungal Therapies Using Nanomaterials. Nanomedicine, 12(15), 1891–1905. https://doi.org/10.2217/nnm-2017-0052

Oves, M., Arshad, M., Khan, M. S., Ahmed, A. S., Azam, A., & Ismail, I. M. I. (2015). Anti-microbial activity of cobalt doped zinc oxide nanoparticles: Targeting water borne bacteria. *Journal of Saudi Chemical Society, 19*(5), 581–588. https://doi.org/10.1016/j.jscs.2015.05.003

Premanathan, M., Karthikeyan, K., Jeyasubramanian, K., & Manivannan, G. (2011). Selective toxicity of ZnO nanoparticles toward Gram-positive bacteria and cancer cells by apoptosis through lipid peroxidation. *Nanomedicine: Nanotechnology, Biology and Medicine*, 7(2), 184–192. https://doi.org/10.1016/j.nano.2010.10.001

Ravi, A., Samuel, J., Sahaya Jude Dhas, S., Usharani, S., Simon, T., Senthil Kumar, D., Jasmin Vijith, S. K., Sivakumar, A., Suresh Kumar, R., & Biju, C. S. (2024). Structural,

morphological, optical and antibacterial performances of rare earth (Sm)-doped ZnO nanorods. *Journal of Rare Earths*. Advance online publication. https://doi.org/10.1016/j.jre.2024.01.004

Santos, A. C., Morais, F., Simões, A., Pereira, I., Sequeira, J. A. D., Pereira-Silva, M., Veiga, F., Ribeiro, A. J. (2019). Nanotechnology for the development of new cosmetic formulations. *Expert Opinion on Drug Delivery, 16*(4), 313–330. https://doi.org/10.1080/17425247.2019.1585426

Schiavo, L., Cammarano, A., Carotenuto, G., Longo, A., Palomba, M., & Nicolais, L. (2024). An overview of the advanced nanomaterials science. *Inorganica Chimica Acta, 559,* 121802. https://doi.org/10.1016/j.ica.2023.121802

Sharma, N., Jandaik, S., Kumar, S., Chitkara, M., & Sandhu, I. S. (2016). Synthesis, characterisation and antimicrobial activity of manganese- and iron-doped zinc oxide nanoparticles. Journal of Experimental Nanoscience, 11(1), 54–71. https://doi.org/10.1080/17458080.2015.1025302

Sharma, R. K., & Ghose, R. (2015). Synthesis of zinc oxide nanoparticles by homogeneous precipitation method and its application in antifungal activity against Candida albicans. *Ceramics International*, 41(1, Part B), 967–975. https://doi.org/10.1016/j.ceramint.2014.09.016

Shukla, S., & Sharma, D. K. (2020). A review on rare earth (Ce and Er)-doped zinc oxide nanostructures. *Materials Today: Proceedings*. https://doi.org/10.1016/j.matpr.2020.05.264

Sushma, C., & Kumar, S. G. (2017). Advancements in the zinc oxide nanomaterials for efficient photocatalysis. *Chemical Papers, 71*, 2023–2042. https://doi.org/10.1007/s11696-017-0217-5

Subash, B., Krishnakumar, B., Swaminathan, M., & Shanthi, M. (2013). Synthesis and characterization of cerium–silver co-doped zinc oxide as a novel sunlight-driven photocatalyst for effective degradation of Reactive Red 120 dye. *Materials Science in Semiconductor Processing, 16*(4), 1070–1078. https://doi.org/10.1016/j.mssp.2013.04.001

Yougbaré, S., Mutalik, C., Okoro, G., Lin, I. H., Krisnawati, D. I., Jazidie, A., ... & Kuo, T. R. (2021). Emerging trends in nanomaterials for antibacterial applications. *International Journal of Nanomedicine, 16*, 5831–5867. https://doi.org/10.2147/IJN.S328767

Zhang, J., Tian, B., Wang, L., Xing, M., & Lei, J. (2018). *Photocatalysis*. Lecture Notes in Chemistry. Springer. https://doi.org/10.1007/978-981-13-2113-9

Zheng, B., Fan, J., Chen, B., Qin, X., Wang, J., Wang, F., Deng, R., & Liu, X. (2022). Rare-earth doping in nanostructured inorganic materials. *Chemical Reviews, 122*(6), 5519–5603. https://doi.org/10.1021/acs.chemrev.1c00644